AD-A150 944 EXPERIMENTAL INVESTIGATION OF NEUTRAL PLASMA BEAM PROPAGATION ACROSS A MA..(U) AMAF INDUSTRIES INC COLUMBIA MD C SPIGHT ET AL. 23 SEP 84 8409-X1300-200 1/1

UNCLASSIFIED AFOSR-TR-85-0097 F49620-83-C-0091 F/G 20/9 NL

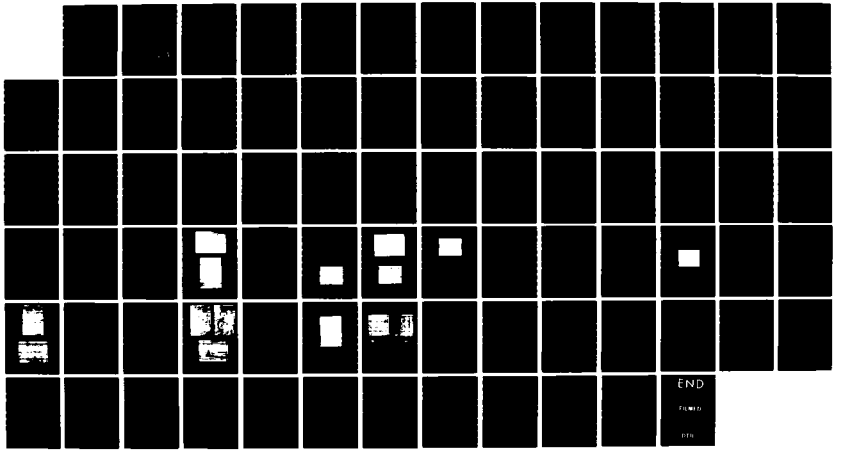

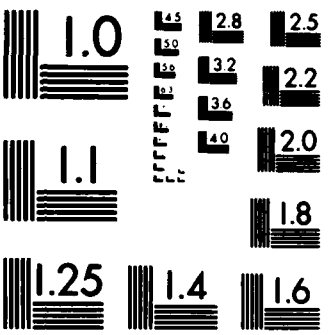

MICROCOPY RESOLUTION TEST CHART
NATIONAL BUREAU OF STANDARDS-1963-A

AFOSR-TR- 85-0097

(2)

FINAL REPORT
FOR
EXPERIMENTAL INVESTIGATION OF NEUTRAL PLASMA BEAM PROPAGATION ACROSS A MAGNETIC FIELD

AMAF Industries Incorporated

Contract No. F49620-83-C-0091
AMAF Report No. 8409-X1300-200

FINAL REPORT
FOR
EXPERIMENTAL INVESTIGATION OF NEUTRAL PLASMA BEAM PROPAGATION ACROSS A MAGNETIC FIELD

Submitted to

Directorate of Physical and Geophysical Sciences
Air Force Office of Scientific Research
Bolling Air Force Base
Washington, D.C. 20332

Prepared by

AMAF Industries, Inc.
9052 Old Annapolis Road
Columbia, Maryland 21045

REPORT DOCUMENTATION PAGE		READ INSTRUCTIONS BEFORE COMPLETING FORM
1. REPORT NUMBER AFOSR-TR- 85-0097	2. GOVT ACCESSION NO. AD-A150 944	3. RECIPIENT'S CATALOG NUMBER
4. TITLE (and Subtitle) Experimental Investigation of Neutral Plasma Beam Propagation Across a Magnetic Field		5. TYPE OF REPORT & PERIOD COVERED Final Report 6. PERFORMING ORG. REPORT NUMBER
7. AUTHOR(s) Dr. Carl Spight/Robert W. Miller		8. CONTRACT OR GRANT NUMBER(s) F49620-83-C-0091
9. PERFORMING ORGANIZATION NAME AND ADDRESS AMAF Industries, Inc. 9052 Old Annapolis Road Columbia, Maryland 21045		10. PROGRAM ELEMENT, PROJECT, TASK AREA & WORK UNIT NUMBERS N/A
11. CONTROLLING OFFICE NAME AND ADDRESS Air Force Office of Scientific Research Building 410 Bolling AFB, D.C. 20332		12. REPORT DATE September 23, 1984 13. NUMBER OF PAGES
14. MONITORING AGENCY NAME & ADDRESS(if different from Controlling Office) DCASMA-Baltimore 300 East Joppa Road Hampton Plaza Building, Room 200 Towson, Maryland 21204		15. SECURITY CLASS. (of this report) Unclassified 15a. DECLASSIFICATION/DOWNGRADING SCHEDULE

16. DISTRIBUTION STATEMENT (of this Report)

Approved for Public Release; Distribution Unlimited

17. DISTRIBUTION STATEMENT (of the abstract entered in Block 20, if different from Report)

N/A

18. SUPPLEMENTARY NOTES

19. KEY WORDS (Continue on reverse side if necessary and identify by block number)

Diagnostic
Current
Magnetic Field
Plasma (Physics)
Plasmoid

20. ABSTRACT (Continue on reverse side if necessary and identify by block number)

(SEE NEXT PAGE)

The conversion, described herein, of a pre-existing Hypervelocity Plasma Generator Facility to operate in a regime of importance to particle beam research has been completed. The facility is now capable of producing a plasma flow-magnetic field environment that in a scaled manner simulates the exoatmospheric propagation of a plasmoid across the geomagnetic field. A full set of flow and field diagnostics have been implemented and calibrated. It includes magnetic field probes for the slowly varying transverse background and the fast varying motionally induced fields, a laser schliren system for monitoring density gradient structure of the beam and time-of-flight fast photodiode probes for beam velocity measurements. Port access is available for monitoring directly electrostatic or electromagnetic fields associated with beam propagation. In tandem with experimental activity a theoretical analysis effort has been initiated, in interaction with theoreticians at Los Alamos Scientific Laboratory, which intends a significant contribution to the stability analysis of a bounded plasma beam which can exhibit polarization and/or diamagnetic effects. No satisfactory theory or numerical simulations are currently available for that intrinsically three-dimensional dynamics.

Complete supplied keywords included. → to front

TABLE OF CONTENTS

1.0 INTRODUCTION

There is an extensive literature, spanning more than four decades, describing investigations of spatially localized streams or plasma-magnetic field entities (plasmoids) in interaction with background magnetic field environments. Those investigations include theoretical analyses, computer simulations, and experimental research efforts. The large fraction of these investigations, however, have concerned plasma interactions characterized by $M_A \lesssim 1$, where M_A is the Alfven mach number defined such that:

$$M_A^2 = (\text{plasma flow velocity/Alfven speed})^2$$
$$= (\text{plasma kinetic energy density})/(\text{magnetic field energy density})$$

It is well established that in such regimes, the plasma is either strongly decelerated (and/or trapped) by the transverse magnetic field or propagates unimpeded (only after undergoing charge polarization effects) at the reduced ExB drift velocity. Very little work has been done in the "super-Alfvenic" regimes: $M_A >> 1$. This is the regime of critical importance in the exoatmospheric propagation of very energetic neutralized charged particle beams. Recent computer simulations in that regime (e.g., those of the theory group effort at Los Alamos Scientific Laboratory (LASL)) have shed some light on propagation dynamics but have been handicapped by the following limitations:

a. The lack of any clearly justifiable choice criteria for selecting among the many possibilities for collective mode instabilities in that growth rates depend critically upon assumed initial plasma flow structures.

b. The computational complexity and time intensivity of full three-dimensional simulations necessary to treat correctly the boundary effects which are inescapable in actual beam propagation.

c. The limited ability to follow the plasmoid for long (simulation) propagation distances (related to computer memory size/computation time limitations) and/or the inability to choose rationally among possible computation box boundary conditions.

d. An absence of knowledge of the significance of nonlinear processes in either saturating linearly growing instabilities or aggravating their effect.

Associated theoretical efforts have almost always been restricted to linearized treatments and/or have assumed (for tractability) highly simplified geometries.

It that light, a carefully organized set of scaled simulation experiments can thus provide important new knowledge which can support and complement the theoretical and computer simulation efforts. This is the significance of the effort supported by the contract (F49620-83-C-0091) now ended. The experimental facility which was used is located at Morehouse College, Atlanta, Georgia and was made available to AMAF Industries, Inc. on a leased basis.

2.0 STATEMENT OF WORK

The research objectives for the effort as proposed were defined by the following tasks:

1. Establish effective channel of communications with existing computer simulation groups (e.g., LASL).

2. Review published literature on experimental and theoretical research on instabilities in the plasma flow regime $M_A \lesssim 1$ for applicable insights.

3. Reconfigure existing hypervelocity plasma flow generator facility to operate with high reproducibility in the regime $M_A >> 1$ as well as $M_A \gtrsim 1$.

This will involve (as simple engineering tasks):

a. Extension of the vacuum chamber in the flow direction by addition of a four-foot pyrex glass pipe section.

b. Redesign and reconstruction of the magnetic field producing coil system (currently a Helmholtz pair) to produce an approximately uniform field over the extended flow channel.

c. Addition of a ballast chamber, a precision leak valve, a mechanical vacuum pump, and a vacuum gauge to supply controllable quantities of selected gases to the breech of the gun (operating in the gas "puff" mode).

4. Construct and calibrate fast response magnetic, electric and current probes for flow diagnostics (designed by well-known techniques, to have response time $\lesssim 0.1$ μsec).

5. Procure and bring to operational status a fast optical system (image convertor or Kerr optics) for macroscopic structure observations.

6. Begin program of experimental parmetric surveys (with full diagnostic monitoring):

a. Plasma beam velocity.

b. Plasma beam density.

c. Plasma beam particle mass (variations in composition).

d. Propagation chamber ambient pressure.

e. Background magnetic field intensity.

f. Background magnetic field structure.

7. Analyze results of experimental surveys as to:

a. Dependence of propagation stability on parameter values.

b. Characteristic of instability structure (growth rates, spatial scales, onset conditions, saturation levels).

8. Summarize results in form for inclusion in computer simulations (especially in computer simulation areas a. and d. described previously).

9. Investigate experimentally (guided by appropriately modified LASL computer code predictions as they become available) possible means for stabilizing the propagating beam with an aim of achieving the highest energy in the beam consistent with stability.

3.0 REVIEW OF PREVIOUS RESEARCH RELEVANT TO NEUTRAL PLASMA BEAM PROPAGATION ACROSS A MAGNETIC FIELD

This review of previous research relevant to plasmoid propagation is intended to serve a number of purposes. Firstly, it presents results from previous research which expounds some of the problems encountered in analyzing plasmoid propagation. Secondly, it aids in the construction of a foundation of basic concepts which must be utilized in discussing plasmoid propagation. Lastly, it serves to motivate new approaches to analyze plasmoid propagation with the contention that many of the previously obtained results cannot be utilized in current analyses of plasmoid propagation.

To begin the review, it should be noted that previous research relevant to plasmoid propagation was concerned with a wide variety of applications, ranging from the interaction of the solar wind with the geomagnetic field to the injection of pulsed, neutralized ion beams into devices designed to achieve thermonuclear fusion. This wide variety of applicability has presented problems to those with present interests in plasmoid propagation in the sense that it becomes difficult to extract pertinent information due to the disparate parameter regimes involved. It thus becomes necessary to carefully inspect previous analyses to determine which parameter regimes are relevant to present interests in plasmoid propagation (i.e. military applications).

Another problem associated with employing results from previous research are the limitations imposed by the highly idealized geometric configurations that were considered. For example, Ferraro [1], concerned with the origin of geomagnetic storms, was able to analytically describe the case of a diamagnetic effect - dominated semi-infinite plasma-field interaction. The limitation in this case being the absence of finite geometry (boundary) effects on the diamagnetic current flow patterns. Also, the analysis performed by Ferraro was essentially time-independent, which for present applications is unsuitable.

It can be stated however, that Ferraros' analysis did provide certain contributions that aided in the understanding of plasmoid propagation. Ferraro, concerned primarily with the case of a plasma flow with sufficient kinetic energy density to exclude the ambient magnetic field, demonstrated that the magnetic field decayed within a distance "$c/\omega p$" of the surface of the plasma. The quantity "$c/\omega p$", known as the "collisionless skin depth" where "c" is the velocity of light and "ωp" is the electron plasma frequency, is on the order of kilometers for the solar wind and on the order of a centimeter for high density plasmas of interest for military applications.

Ferraro has shown that magnetic field exclusion can be expected to occur when the square of the Alfven Mach number

(Ma^2), defined as the ratio of plasma kinetic energy density to magnetic field energy density, is much greater than one; (i.e. $Ma^2 >> 1$). For plasmoids relevant to military applications, the ratio (Ma^2) is on the order of 10^{10} and thus serves as an important parametrical guideline.

To justify the importance of the parameter (Ma^2), it becomes necessary to trace the expected sequence of events in the flight of a plasmoid entity. From the aforementioned kinetic energy density considerations, one is lead to expect that the initial phase of flight is dominated and thus characterized by magnetic field exclusion from the interior of the plasmoid. The field exclusion is produced by diamagnetic currents circulating in the thin surface layer of the plasmoid. These circulating diamagnetic currents will eventually decay due to classical, discrete particle Spitzer[2] conductivity and also possibility due to enhanced anomolous resistivity induced by non-linear instabilities driven by the diamagnetic currents. Thus, the decay of these diamagnetic currents permits partial diffusion of the magnetic field into the plasmoid after the initial phase of propagation. An estimate for the diffusion time τ_D can be obtained from the approximation:

$\tau_D = 4\pi\sigma L^2/C^2$ where σ is the plasmoid conductivity and L is a scale length. For plasmoids with particle densities and kinetic energy densities relevant to military applications, and

assuming Spitzer conductivity, one obtains $\tau_D \simeq 1$ micro-second. When considering the expected time-of-flights for military applications, and the possible enhancement of anomolous resistivity, one can conclude that the magnetic field will partially permeate the plasma throughout the majority of flight. This conclusion has lead to the development of several analytical models, attempting to describe and/or simulate plasmoid propagation in parameter regimes relevant to military applications, which employ the concept of a polarized plasma propagating across a magnetic field through an E x B drift of plasma particle guiding centers. The validity of these models is questionable, however, since many ignore the strong plasma heating which may occur during the initial diamagnetic phase of propagation. It is therefore the intention of the next section of this report to expound the limitations inherent in such models; examples of which include:

3.1 MODEL 1: WILLIAM PETER AND NORMAN ROSTOKER

The objective of this model is to provide a theoretical basis for the injection of pulsed, neutralized ion beams into toroidal fields for the purpose of driving currents[3] or of supplementary tokamak heating.[4] This model considers only the case of $R \lesssim a_i$, where R is the plasma beam radius and a_i is the ion gyro-radius, such that space-charge polarization is induced on the edges of a bounded plasma column

as it passes through a transverse magnetic field. The polarization space charge layers create a self-consistent electric field which allows the plasmoid to propagate across the magnetic field by means of the E x B drift. The criteria and/or assumptions which characterize the conditions for this motion to take place are as follows:

3.1.1 The plasma beam must have sufficient kinetic energy to create the polarization electric field. In analytical terms,

$$1/2\ n_o M u_o^2 >> \frac{Ey^2}{8\pi}$$

where n_o and U_o are the initial density and velocity of the plasmoid, M is the ion mass, and Ey is the polarization field. It is further required in this model that the plasma drift across the transverse magnetic field lines with its initial forward velocity U_o, which implies that;

$$\omega_{pi}^2 >> \Omega_i^2 \quad \text{or} \quad \epsilon = 1 + \frac{\omega_{pi}^2}{\Omega_i^2} >> 1$$

where ω_{pi} is the ion plasma frequency, Ωi is the ion gyrofrequency and ε is the static plasma dielectric constant.

3.1.2 A low beta (β) plasma is assumed such that the magnetic field due to induced plasma currents is negligible.

Beta, defined as the ratio of plasma particle pressure to magnetic field pressure, indicates the amount of influence diamagnetic effects have on the plasmoid propagation.

3.1.3 The plasmoid motion is assumed non-adiabatic, which implies the more general 2-fluid equations of motion must be utilized.

3.1.4 All physical variables, such as density and velocity, are assumed to be functions of the longitudinal coordinate and time only.

3.1.5 Plasma quasi-neutrality is assumed such that the ion density (n_i) equals the electron density (n_e) (i.e.; $n_i \simeq n_e \simeq n$) where n is a common density called the plasma density.

These assumptions form the foundation upon which the analytics of this model are based. Without belaboring the details of these analytics, a review of the quantitative results produced by this model is necessary. This review will enable comparison of results produced from other plasmoid propagation models.

As a starting point, a schematic drawing of the polarization of a bounded plasma beam in a transverse magnetic field B_z is presented in Figure 1. Note the coordinate configuration

in which the plasmoid propagates in the $\hat{x}$ direction. Note also that Δy represents the width of the polarization charge layers. The analytical solutions for plasmoid position (x) and velocity (U_x) derived for this configuration, neglecting terms of order ($1/\epsilon^2$), are:

$$[1] \quad U_x \simeq U_o \left\{ 1 - \frac{1}{\epsilon} \left[1 - \cos\sqrt{\epsilon}\Omega_H \left(t + \frac{x_o}{U_o} \right) \right] \right\}$$

and

$$[2] \quad X = U_o \left\{ \left(t \times \frac{x_o}{U_o} \right) \left(1 - \frac{1}{\epsilon} \right) + \frac{1}{\epsilon^{3/2}\Omega_H} \operatorname{Sin} \left[\epsilon\Omega_H \left(t + \frac{x_o}{U_o} \right) \right] \right\}$$

where:

x_o = initial plasmoid position for t = 0.

U_o = initial plasmoid velocity for t = 0.

Ω_H = hybrid gyrofrequency = $(\Omega_i \Omega_e)^{1/2}$.

ϵ = static plasma dielectric constant.

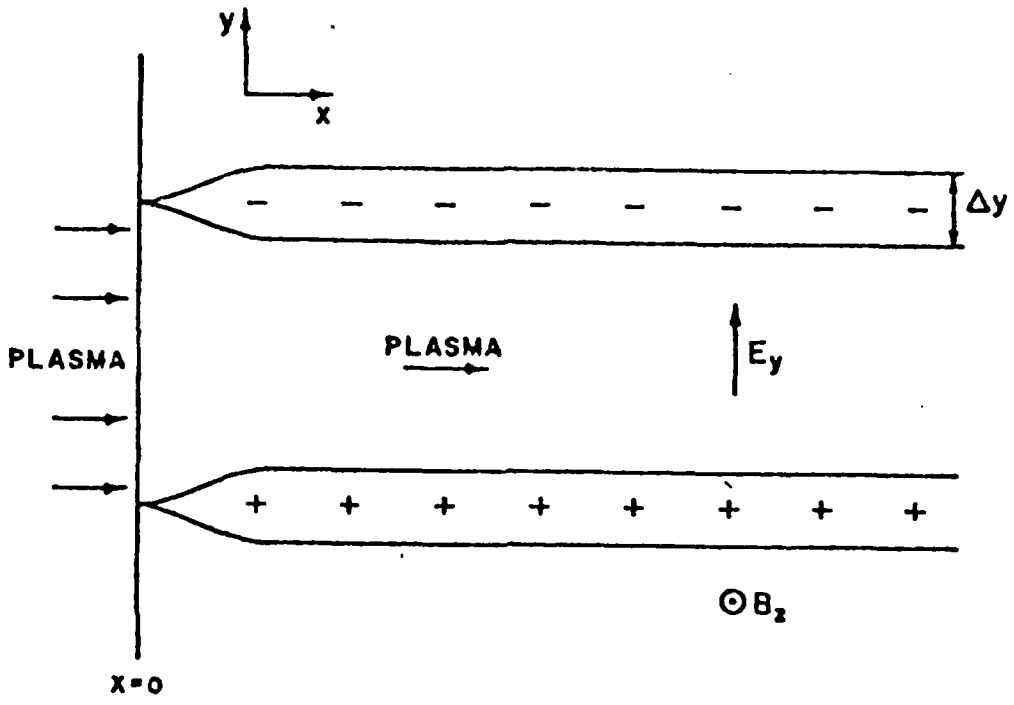

FIGURE 1. Schematic drawing of the polarization of a bounded plasma beam in a transverse magnetic field B_z. The resultant electric field E_x allows the beam to propagate through the magnetic field by means of an EXB plasma drift.

The oscillatory behavior of the plasmoid velocity in equation [1] is due to competing effects of the polarization electric field and the transverse magnetic field. The frequency of oscillation, $\sqrt{\epsilon\ \Omega_H}$, is the electron plasma frequency ω_{pe} for $\epsilon >> 1$. Note that the solutions are valid for small values of ϵ (i.e.; $\epsilon \lesssim (M/m)^{1/2}$) although the quasi-neutrality assumption is no longer valid in this parameter regime. For a value of ϵ equal to unity, the resulting charge distribution is unable to generate a polarization electric field sufficient to allow propagation. In this case, the plasmoid propagates across the transverse magnetic field to a scale length equal to the hybrid gyroradius a_H and is reflected back to the injection plane. An expression for the mean plasma velocity $\bar{U}_x$ can be obtained by averaging out the fast time oscillations in equation [1]. The result is:

$$[3] \quad \bar{U}_x = U_o \left(1 - \frac{1}{\epsilon}\right)$$

For large values of ϵ (i.e.; $\epsilon >> 1$), it can be seen from equation [1] that the plasmoid will propagate across the magnetic field with a velocity nearly equal to its injection velocity U_o. In the limit $\epsilon >> 1$, the equations [1] and [2] reduce to, respectively;

$$[4] \quad U_x = U_o \left\{ 1 - \frac{1}{\epsilon} \left[1 - \cos \frac{\sqrt{\epsilon}\, x}{a_H} \right] \right\}$$

$$[5] \quad X \simeq U_o \left[t + \frac{X_o}{U_o} \right]$$

which is exactly the steady state solution derived by Sinelnikov and Rutkevich in the "slow-deceleration approximation" to be discussed in the next section.

Before discussing the "slow-deceleration approximation," however, it is worthwhile to investigate quantitatively, limiting values of ϵ and its implications on the plasmoid propagation. For ϵ=1, we have found that the plasmoid transverses the magnetic field lines to scale length equal to the hybrid gyroradius (a_H) and is then reflected back to the injection plane, for ϵ=10, the plasmoid undergoes large oscillations, and for ϵ =100, the plasmoid undergoes smaller oscillations. This is depicted graphically in Figure 2. It should be noted that the solution for the plasmoid velocity U_x expressed in equation [4] is valid for $\epsilon >> 1$, however, there lies a further restriction on the value of ϵ limiting the validity of this model. Due to the quasi-neutrality assumption; it has been derived that, the domain of validity of this model is restricted to $\epsilon >> (M/m)^{1/2}$. If this condition is not satisfied, it is expected that longitudinal, as opposed to transverse, space charge polarization effects will be dominant.

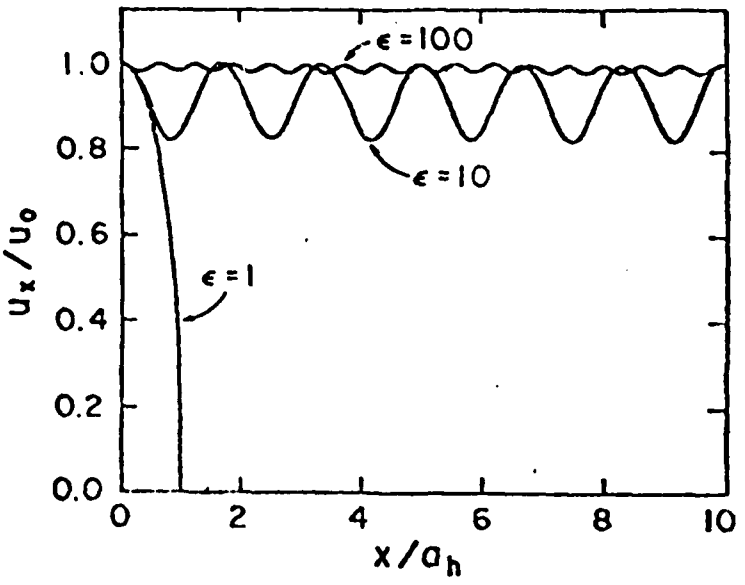

Plots of longitudinal velocity U_x/U_o versus distance x/a_h into the field for three different values of the plasma dielectric constant ϵ.

FIGURE 2. PLASMOID OSCILLATIONS

It is obvious that the plasma oscillations depicted in Figure 2 cannot be sustained indefinitely, thus, one must take into account the expected damping of these oscillations by introducing a collisional term into the species (e,i) equations of motion. Using the Langevin[5] description for the collision frequency, a term proportional to $\nu(V_i - V_e)$ has been introduced, and the result is that the plasma oscillations damp out after a few hybrid gyroperiods ($\Omega_H = \left[\Omega_i \Omega_e\right]^{1/2}$).

Finally, to complete the review, a more critical analysis of the limitations of this model and their implications is necessary. Firstly, an important limitation of this model is its inability to describe the formation of the polarization space-charge layers. Secondly, a more complete model would consider a truly bounded plasma column, with the physical variables, such as density and velocity, being functions of the planar coordinates perpendicular to the magnetic field direction. In actuality, these physical variables are three-dimensional. Thirdly, the extent to which this model considers longitudinal space-charge polarization effects is limited in the sense that the only results yielded by this model that are relevant to these considerations is that the condition $\epsilon >> (M/m)^{1/2}$ corresponds to the characteristic distance for transverse charge separation (a_i/ϵ) being less than the characteristic distance for longitudinal charge separation $(a_i a_e)1/2$. Lastly, because this model considers low-beta plasmas only, there also exists an upper limit on the values that the static plasma dielectric constant ϵ can have. From the relation $\beta = (U_o^2/C^2)\epsilon << 1$, we have the condition that $\epsilon << (U_o^2/C^2)^{-1}$. Thus the limiting values of ϵ are; $(M/m)^{1/2} << \epsilon << (U_o^2/C^2)^{-1}$. An explanation for the higher threshold $\epsilon >> (M/m)^{1/2}$ required for cross-field propagation in this model as opposed to the adiabatic condition $\epsilon >> 1$ derived by Schmidt[6], is that in this model, the plasma column enters the applied

magnetic field from an initial field-free region; whereas the condition $\epsilon >> 1$ applies to plasmas moving initially within a magnetic field region.

3.2 MODEL 2: K.D. SINEL'NIKOV AND B.N. RUTKEVICH

The objective of this model is to provide a theoretical basis for describing the propagation of a bounded plasma flux in a magnetic field with special emphasis on the formation of transverse and longitudinal polarization space-charge layers. The transverse polarization space-charge layers create a self-consistent electric field ($\vec{E}_T$) which allows the plasmoid to propagate across the magnetic field by means of the $\vec{E}_T \times \vec{B}$ drift. The longitudinal polarization space-charge layers create a self-consistent electric field ($\vec{E}_L$) which may lead to plasmoid reflection back to the injection plane depending on the value of the static plasma dielectric constant ϵ. The criteria and/or assumptions which characterize the conditions for this motion to take place are as follows:

3.2.1 The plasma flux is assumed to be bounded perpendicular to the magnetic field direction ($\vec{B}$) and the plasmoid velocity direction ($\vec{V}$).

3.2.2 Plasma quasi-neutrality is assumed such that the ion density (n_i) equals the electron density (n_e) (i.e.; $n_i \simeq n_e \simeq n$) where n is a common density called the plasma density.

3.2.3 The velocities of the electrons ($\vec{U}_e$) and ions ($\vec{U}_i$) are assumed to be independent of the longitudinal coordinate which is parallel to the direction of plasmoid propagation.

These assumptions form the foundation upon which the analytics of this model are based. Again, without belaboring the details of these analytics, a review of the quantitative results produced by this model is necessary. This review will enable comparison of results produced from other plasmoid propagation models.

As a starting point, suppose that the magnetic field $\vec{B}_z$ on the x=0 plane rises rapidly from zero to a constant value B_z and remains constant for x>0. Plasma bounded in the y direction and consisting of particles of mass m and charges $q = \pm e$ moves along the x axis with velocity U_o, and enters the magnetic field at x=0. Positive and negative particles are deflected in opposite directions along the y axis by the magnetic field $\vec{B}_z$ resulting in a transverse polarization electric field $\vec{E}_T$. Motion of the plasmoid across the magnetic field results from the $\vec{E}_T \times \vec{B}_z$ drift.

In addition to transverse polarization, there exists in this model, longitudinal polarization. Longitudinal polarization results from electrons being deflected by the magnetic field

more than ions. This implies that ions "lead" electrons into the transition layer, due to inertial effects, (i.e.; $M_e << M_i$), resulting in a longitudinal polarization space-charge layer. The resulting electric field $\vec{E}_L$, opposite in direction to the plasmoid velocity, tends to equalize the electron and ion velocities by accelerating the electrons and decelerating the ions such that their penetration depths into the magnetic field are equalized, and thus, removing the space-charge layer discontinuity. Since plasma-quasineutrality is assumed, the relative longitudinal displacements of electrons and ions is considered negligible, however, the resulting electric field $\vec{E}_L$ may be quite large in magnitude since $M_e << M_i$. Also, the plasma-quasineutrality assumption in conjunction with the continuity equation implies that the electron and ion longitudinal velocities are equal. This implication of the quasi-neutrality assumption is justified only if:

a) The electrons <u>do not</u> succeed in describing an appreciable part of the Larmor orbit in a time $\tau \sim 2\pi/\omega_o$; where ω_o equals the plasma frequency.

b) and, the plasma is sufficiently dense.

If the electrons <u>do</u> close their Larmor orbits in a time $\tau \sim 2\pi/\omega_o$, the assumption specified in Section 3.2.3 is no longer valid.

Now that certain aspects on the formation of transverse and longitudinal polarization space-charge layers have been reviewed, a more detailed analysis of the "slow-deceleration approximation" can be performed. As previously mentioned, depending on the value of the plasma dielectric constant ϵ, the plasmoid can be decelerated and then reflected back to the injection plane (i.e.; $\epsilon \gtrsim 1$). For $\epsilon >> 1$, the analytic solution for the plasmoid velocity U_x derived for the "slow-deceleration approximation" is:

$$[6] \quad U_x = U_o \left[1 - \frac{1}{\epsilon} \left[1 - \cos \frac{\omega_o x}{U_o} \right] \right]$$

which is identical to the $\epsilon >> 1$ solution, derived by Peter and Rostoker, presented in Section 3.1. An expression for the mean plasmoid velocity $\bar{U}_x$ can be obtained by averaging out the fast oscillations in equation [6]. The result is:

$$[7] \quad \bar{U}_x \simeq U_o \left[1 - \frac{1}{\epsilon} \right]$$

which implies that the mean plasmoid propagation velocity $\bar{U}_x$ across the magnetic field is <u>not</u> much different that the injection velocity U_o for large values of ϵ.

A graphical depiction of equation [6], which is identical to equation [4], is presented in Figure 2; Section 3.1. The plasma oscillations depicted in this figure cannot be sustained indefinitely, thus one must take into account

the expected damping of these oscillations by introducing a collisional term into the species (e, i) equations of motion. Again, using the Langevin description for the collision frequency, a term proportional to $\nu\vec{v}$, where ν is the effective collision frequency and $\vec{v}$ is the relative velocity of electrons and ions, has been introduced. The result is:

a) if $\nu<2\omega_o$ damped oscillations are obtained; and

b) if $\nu>2\omega_o$ an aperiodic process in which a drift with constant velocity $\bar{U}_x = U_o\ (1-1/\epsilon)$ is established in the course of time.

To complete the review of the "slow-deceleration approximation," it should be mentioned that another important objective of the model was to account for the escape of plasma particles from polarization layers. The escape of plasma particles from polarization layers, which <u>may</u> be due to the flow of plasma along the magnetic lines of force, plays a dominant role in the issues which govern whether or not practical employment of plasma beams can be utilized for exoatmospheric military applications. The escape of particles from polarization layers has an adverse effect on plasma beam directionality and energy flux properties which are two critical issues governing practical employment. Obviously, the mechanism leading

to the escape of particles from polarization layers must be fully understood.

To describe the mechanism, Sinel'nikov and Rutkevich have assumed the plasma beam to be in contact with electrodes joined through a resistance R. By utilizing the energy and momentum balance equations, expressions for the polarization current (I_p), diamagnetic current ($I\mu$), and resistive current (I_R) were obtained. From these expressions, they were able to conclude that the plasma beam was decelerated at the entrance to the space between the electrodes, which lead to an inertial drift current which compensated the current through the resistance R. Consequently, they were able to determine that it is possible for the drift velocity U_x to be very different from the injection velocity U_o, and the energy of transverse motion may be an appreciable fraction of the initial particle energy. The appreciable magnitude of transverse energy could lead to plasma beam dispersal which degrades the directionality and energy flux properties of the plasma beam. If the escape of particles from polarization layers is due to plasma flow along the magnetic lines of force, the compensating current I_R is distributed over the entire thickness of the plasma, as opposed to the narrow layer at the entrance to the space between electrodes, and the conversion of initial particle energy into orbital motion occurs along the entire path of motion along the longitudinal axis. This conversion of energy

into orbital motion again leads to plasma beam dispersal which degrades the directionality and energy flux properties of the beam.

In conclusion, it is our contention that the "slow-deceleration approximation" model formulated by K.D. Sinel'nikov and B.N. Rutkevich is more comprehensive than the W. Peter and N. Rostoker model reviewed in Section 3.1, in the sense that it describes and/or simulates more physical effects characteristic of plasmoid propagation. These physical effects include; actual mechanisms leading to plasmoid propagation across the magnetic field, diamagnetic response, the formation of transverse and longitudinal polarization space-charge layers, the escape of particles from the polarization space-charge layers, and the dissipation of internally circulating diamagnetic currents.

4.0 W. R. SHANAHAN MODEL

This model combines a numerical and analytical study of neutralized plasma beam propagation across a magnetic field. The model addresses physical questions of interest for exo-atmospheric military applications of intense neutralized plasma beams in which attention is focussed on parameter regimes for which the ratio of plasma kinetic energy density to unperturbed magnetic field energy density (Alfven Mach Number; M_a) is large. The review of this model is partitioned into three (3) sections as follows; 1) Numerical, 2) Analytical and 3) Final Results.

4.1 NUMERICAL STUDY

This section serves to review Shanahan's recommended plan of numerical study of plasmoid propagation with special emphasis on the variety of computational tools employed in the study. The general scheme of the numerical study envisioned the application of heuristic, macroscopic considerations and computations to provide initializing data to detailed particle-in-cell (PIC) codes which were utilized to simulate microscopic, phase-space dependent collective phenomena. The results of the PIC simulations were then employed to yield a refined description of plasmoid parameters which enter into the macroscopic treatment with the intention of providing an improved overall description of the plasmoid propagation.

To begin the review, it should be mentioned that there exists a multitude of microscopic phase-space dependent collective effects which can exert a significant effect on the macroscopic behavior of the plasmoid. These microscopic collective effects must be examined on a time scale roughly determined by the reciprocal of the electron plasma frequency ω_{pe}, which for typical parameters is approximately a tenth of a nanosecond, while total times of flight are expected to be several milliseconds. This disparate range of relevant parameters precluded the employment of a single analytic or numerical technique to perform the examination, thus, the present plan of numerical study incorporated a systematic approach employing several techniques. The conceptual trend of the systematic approach, diagrammed in Figure 3, was as follows:

4.1.1 The microscopic features, such as gross charge and current distributions, of the plasmoid were determined through calculations effected with a Magnetohydrodynamic (MHD) fluid numerical code. Classical transport coefficients were employed in this initial phase of the numerical study.

4.1.2 Utilizing the information gained concerning gross charge and current distributions, initialization of PIC simulations was performed to study microscopic, phase-space dependent collective phenomena which can alter the transport coefficients appearing in the MHD fluid description.

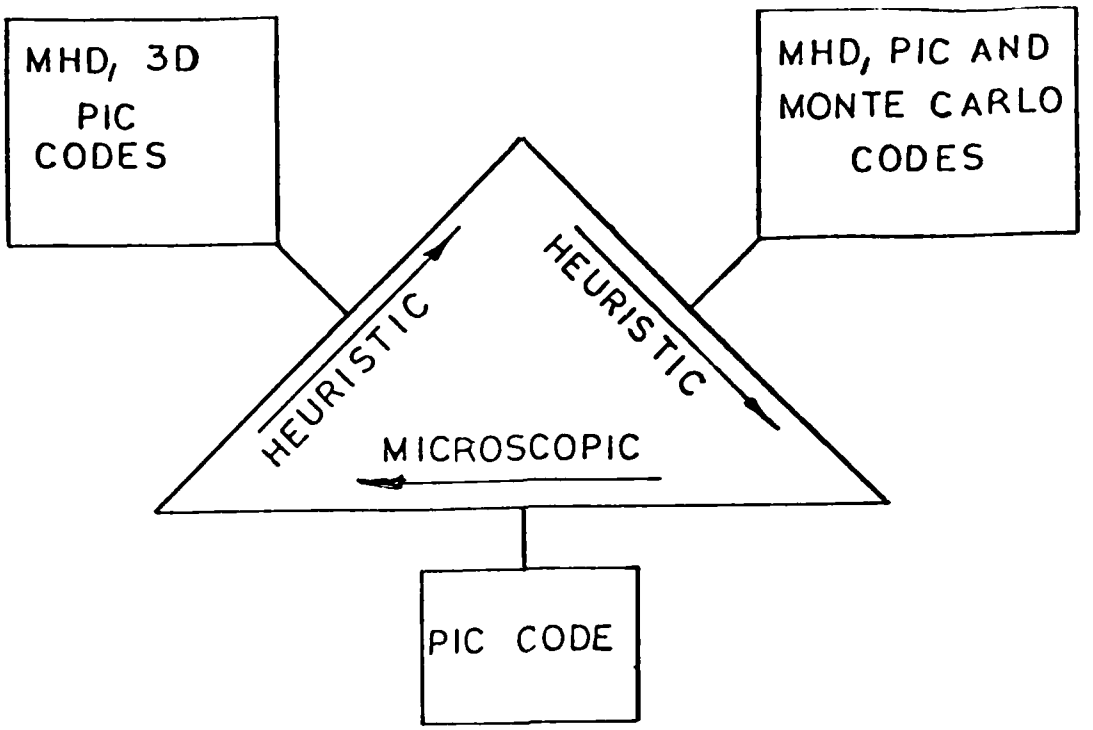

FIGURE 3. THE VARIETY OF COMPUTATIONAL TOOLS EMPLOYED IN THE SYSTEMATIC APPROACH

4.1.3 The effect of discrete interactions of plasmoid particles with a background neutral gas was then investigated through employment of a Monte Carlo transport code. The particular Monte Carlo code employed in the present numerical study included the effect of an externally prescribed, but not self-consistent, electromagnetic field on the trajectories of the plasmoid particles. By employing the Monte Carlo code with a variety of initial conditions, it was determined qualitatively, what effects background interactions have on the plasmoid distribution function. Data acquired from the Monte Carlo calculations was then employed

to initialize the PIC simulation code. The objective of performing PIC simulations with initializing Monte Carlo data was to evaluate the effect of the collective, restorative forces neglected in the Monte Carlo calculations.

4.1.4 Insight gained concerning anomalous, collectively induced transport effects would then be applied to yield a refined, accurate description of the macroscopic aspects of neutral plasma beam propagation across a magnetic field.

Now that the basic conceptual trend of the present numerical study has been reviewed, it is worthwhile to describe the various computational tools employed.

The principal numerical code employed in the present study of an intense neutralized plasma beam propagating across a magnetic field was CCUBE, a two-dimensional, relativistic, fully electromagnetic particle-in-cell simulation code. CCUBE can be applied to study plasmoid configurations in any orthogonal curvilinear coordinate system. By employing CCUBE in the heuristic mode, it is meant that the plasmoid is simulated as a whole, as opposed to specific region such as an ion sheath in which diamagnetic currents may flow.

Heuristic, fluid calculations were effected with two magnetohydrodynamic (MHD) codes. A two-dimensional, Eulerian

code proved to be the most useful in the present numerical study due to the inherent features of the code such as the inclusion of phenomological resistivity, energy loss due to bremsstrahlung and line radiation, and a moving reference frame option. The second MHD code employed was a two-dimensional Lagrangian code applicable to problems with fluid-vacuum and fluid-fluid interfaces. The inclusion of phenomological resistivity was also a feature of this code.

Calculations concerning the interactions of plasmoid particles with background neutral gas atoms were effected with the code CYLTRAN. This code computes electron, ion and photon transport consistently with the presence of an externally prescribed electromagnetic field. The code CLYTRAN is actually an embodiment of several Monte Carlo techniques.

Before completing this review of Shanahan's numerical study of plasmoid propagation, it is necessary to describe the limitations inherent in the various computational tools employed. Firstly, no detailed particle dynamics are included in the MHD fluid codes, which implies that in determining the gross charge and current distributions, the transport coefficients must be pre-specified. Arbitrary, but reasonable values for these coefficients are supplied by using the collisional Spitzer values. Obviously, supplying incorrect values would lead to erroneous results.

For example, providing a value of the conductivity derived from the Spitzer formula could lead to a much smaller Joule heating, and accompanying plasmoid dispersal, than that obtained from a more realistic, collectively enhanced (anomalous) electrical resistivity[2]. Since the principal quantity to be evaluated in Shanahan's numerical study is the collectively enhanced resistivity, which can be determined only by detailed microscopic calculations, a cyclic nature is established within the study and is depicted in Figures 4 and 5. It cannot be over emphasized that it is absolutely critical to obtain a refined, accurate value for the collectively enhanced resistivity in order to understand the mechanisms leading to plasmoid dispersal, which is one of the major issues governing whether or not practical employment of intense neutralized plasma beams for military purposes is possible. Secondly, restrictions on the applicability of MHD fluid codes and PIC simulation codes arise essentially from the two-dimensional nature of the codes. Various restrictions include; the inability to vary the magnetic field in the third dimension, possible magnetic field exclusion from the path of the plasmoid is not permitted, current may flow freely in the third dimension, and consequently the magnetic field continues to increase

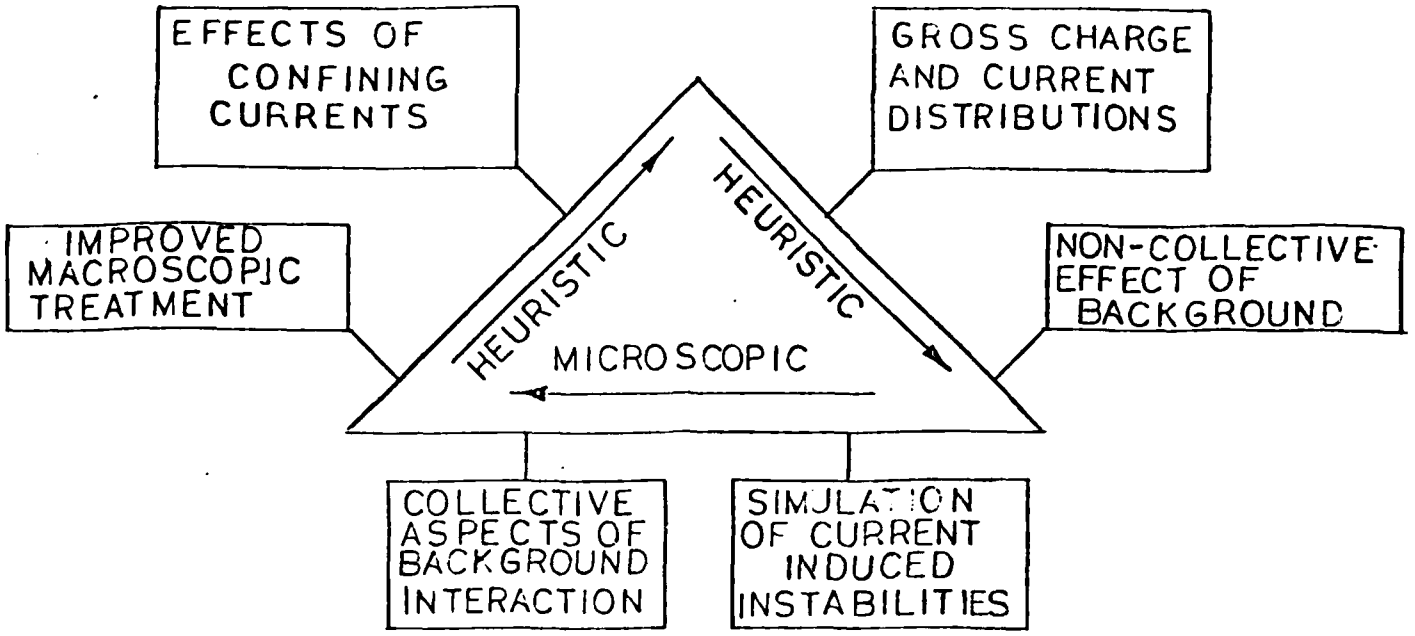

FIGURE 4. A NUMERICAL STUDY COMBINING HEURISTIC, MACROSCOPIC MODELLING WITH MICROSCOPIC, PARTICLE-IN-CELL SIMULATIONS

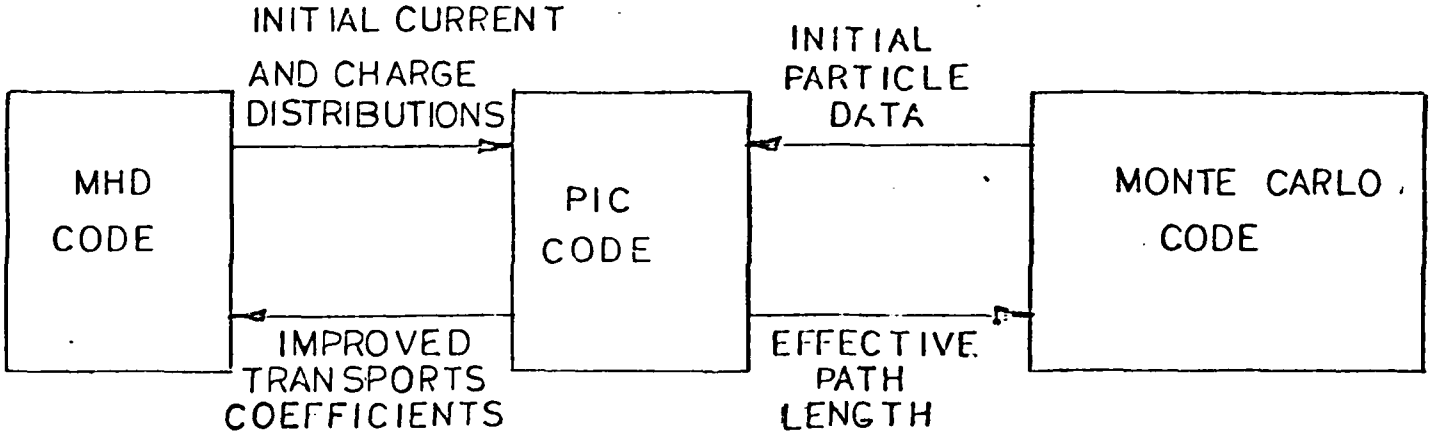

FIGURE 5. A REINFORCING CYCLIC FLOW OF INFORMATION BETWEEN THE HEURISTIC MODELLING AND THE MICROSCOPIC, PARTICLE-IN-CELL SIMULATIONS

in the precursor region of the plasmoid. Lastly, in the PIC simulation, a neutral plasma beam is injected into a computational box with specified boundaries containing a transverse magnetic field. The specified boundaries limit the plasmoid time of transit and in turn limit the time of simulation. Also, the physical dimensions of the plasmoid must be chosen to facilitate fitting the plasmoid into the computational mesh without loss of desired resolution.

4.2 ANALYTIC STUDY

The objective of the present analytic study was to derive an expression for the dynamic magnetic field response within the context of a simple plasmoid slab model. Self-consistent coupling of this response to the plasmoid equations of motion revealed the excitation of collective oscillations. These collective oscillations, due to initial charge separation, leads to significant plasmoid heating which causes plasmoid dispersal. The dynamic magnetic field response within the context of a simple slab model was derived as follows:

4.2.1 Model plasmoid as slab of width L in x-direction, but uniform in two transverse directions.

4.2.2 Permit field quantities to vary in one perpendicular direction.

4.2.3 Derive equation for dynamic magnetic field response.

a. Basic wave equation

$$\Delta^2 A_z - \frac{1}{c^2} \frac{\partial^2 A_z}{\partial t^2} = -\frac{4\pi}{c} j_z \qquad (1)$$

b. Obtain expression for current (j_z) from conservation of canonical angular momentum.

$$j_z = \frac{\omega p^2}{4\pi c\gamma}\left[A_o(X_o) - A_z(X)\right] \qquad (2)$$

where

$$X_o \simeq X - V_o t$$

c. Combine with the basic wave equation to obtain the desired equation.

$$\left[\frac{\partial^2}{\partial X^2} - K_o^2 - \frac{1}{c^2}\frac{\partial^2}{\partial t^2} - \frac{\omega p^2}{c^2\gamma}\right] A_z = \frac{\omega p^2}{c^2\gamma} B_o (X - V_o t) \qquad (3)$$

4.2.4 Solve equation (3) as an initial -value problem. Invert Laplace transforms, and evaluate the asymptotic limit ($t \to \infty$) of resultant integrals. Obtain expressions for the dynamic magnetic field response.

a. Precursor

$$B \xrightarrow[L >> c/\omega_p]{} B_0 + \frac{te^{k_o(v_o t - x)}\omega_p^2 B_0 k_0 v_0}{c^2 k_1^2}$$

$$x\left[1 - \frac{k_0}{k_0 + (k_0^2 + \omega_p^2/c^2)^{1/2}}\right]$$

b. Field within Plasmoid slab

$$B \rightarrow B_0 + \frac{t\omega_p^2 B_0 v_0 k_0 k_1}{\left[c^2 k_1^2 (k_0 + k_1)^2 e^{k_1 L} - (k_0 - k_1)^2 e^{-k_1 L}\right]}$$

$$\times \left[(k_0 - k_1) e^{-k_1 L/2} - (k_0 + k_1) e^{k_1 L/2}\right]$$

$$\times \left[e^{k_1 (x - t_0)} - e^{-k_1 (x - v_0 t - L)}\right]$$

c. Wake

$$B \xrightarrow[L >> c/\omega_p]{} B_0 + \frac{te^{k_0 (x + L/2 - v_0 t)} \omega_p^2 B_0 v_0 k_0}{c^2 k_1^2} \left[1 + k_0/k_0 + k_1\right]$$

where:

L = Plasmoid length

W = Plasmoid width

V_o = Initial plasmoid velocity

$K_o = 2\pi/W$

$K_1^2 = K_o^2 + \omega p^2/C^2$

4.3 FINAL RESULTS

The principal results derived from the analytic study were as follows:

a. Wake Region: Magnetic field reversal is exhibited immediately behind the plasmoid.

b. Slab Region: Magnetic field exclusion is exhibited in the plasmoid slab region.

c. Precursor Region: Magnetic field compression is exhibited in the front of the plasmoid.

The principal results derived from the numerical study were as follows:

d. The plasmoid appears to propagate for short distances ($\simeq$ 2 meters) without catastrophic disruption.

e. A longitudinal wave is excited during this period with a wavelength λ = 10cm. The wave excitation within the plasmoid is due to initial charge separation and leads to significant heating in the transverse direction parallel to the magnetic field.

f. Localized heating at the leading edge of the plasma beam is observed causing plasmoid disruption.

Before concluding this review of the Shanahan model of plasmoid propagation across a magnetic field, it is necessary to address inherent problems and/or anomalies associated with the model. Firstly, it is our contention that mathematical errors have propagated throughout the analytic study in the sense that verification of the asymptotic solutions for the dynamic magnetic field response has not been achieved. Secondly, it is our contention that the reference frame transformations utilized in the analytic study, between the laboratory frame and the plasmoid rest frame, are not proper in the sense that the asymptotic solutions for the dynamic magnetic field response exhibit anomalous secularity describing a linear growth in time. Therefore, the Shanahan model, which yields a wealth of information concerning plasmoid propagation across a magnetic field in various parameter regimes, must be carefully analyzed and corrected to ensure absolute validity.

5.0 STATUS OF THE EXPERIMENTAL EFFORT

THE FACILITY CONVERSION:

The facility utilized was located in the Department of Physics at Morehouse College in Atlanta, Georgia. It had previously been used in a Department of Energy sponsored research effort in pulsed, inductive direct energy conversion based on radial expansion flows. The major components of the system are:

A. The coaxial plasma gun and associated capacitor bank.

B. The magnetic field coil system and associated capacitor bank.

C. The vacuum chamber and associated pumps.

D. Plasma and field diagnostics.

F. The data acquisition/control room.

A large area view of the above-table-top-visible portion of the facility is provided in Figures 6a and 6b.

1. The Coaxial Gun and Capacitor Bank - The coaxial plasma gun is a standard Marshall gun configura-

FIGURE 6a

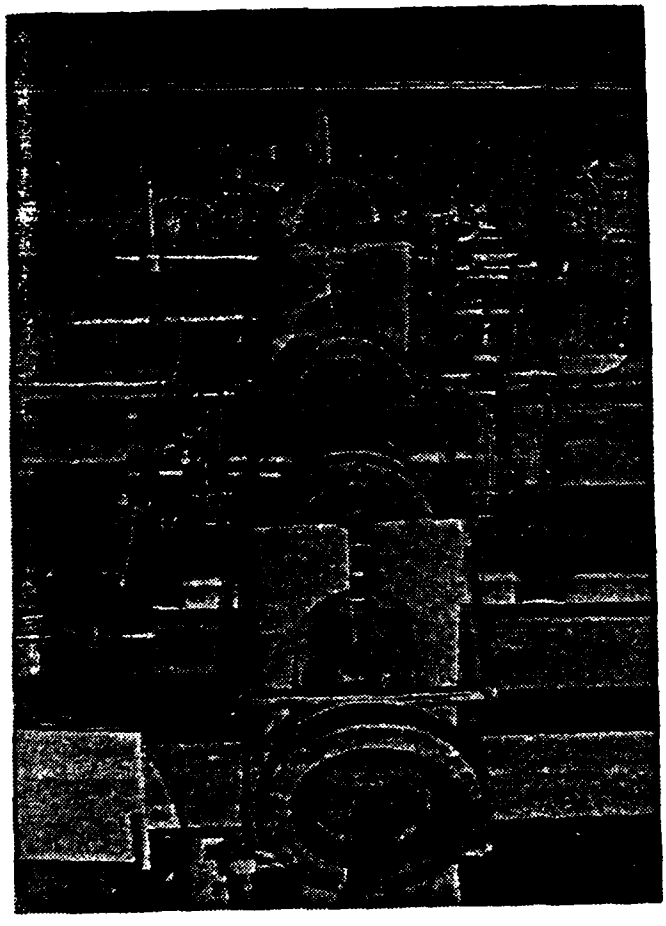

FIGURE 6b

tion capable of being either metallic foil or gas "puff" breech loaded. In the gas "puff" mode, it is loaded by a thyratron controlled, solenoid actuated gas valve. The gun is constructed of copper outer and brass rod inner electrodes with an outer radius/inner radius of 4 and a length of 10 cm. The plasma composition options include He, N, A, or various metals (from foils). Details of the construction of the gun is provided in Figures 7a and 7b. The capacitor bank for the gun is comprised of 8 capacitors rated at 15 uf and 20 KV in parallel yielding a maximum storage of 24 kilojoules. The energy in the bank in switched by 4 type GL-7703 ignitrons in parallel (Figure 8). The capacitor bank switched into the gun has a "ring" frequency of approximately 10 kHz. A typical storage oscilloscope trace of the gun voltage is shown in Figure 9. Nominal plasma densities and flow velocities are respectively $10^{22}m^{-3}$ and 10 km/sec. Figure 10 is an open shutter photograph of the beam.

2. <u>The Magnetic Field Coil System and Capacitor Bank</u> - The transverse magnetic field is produced by a rectangular coil array extending most of the length of the vacuum chamber. The coils

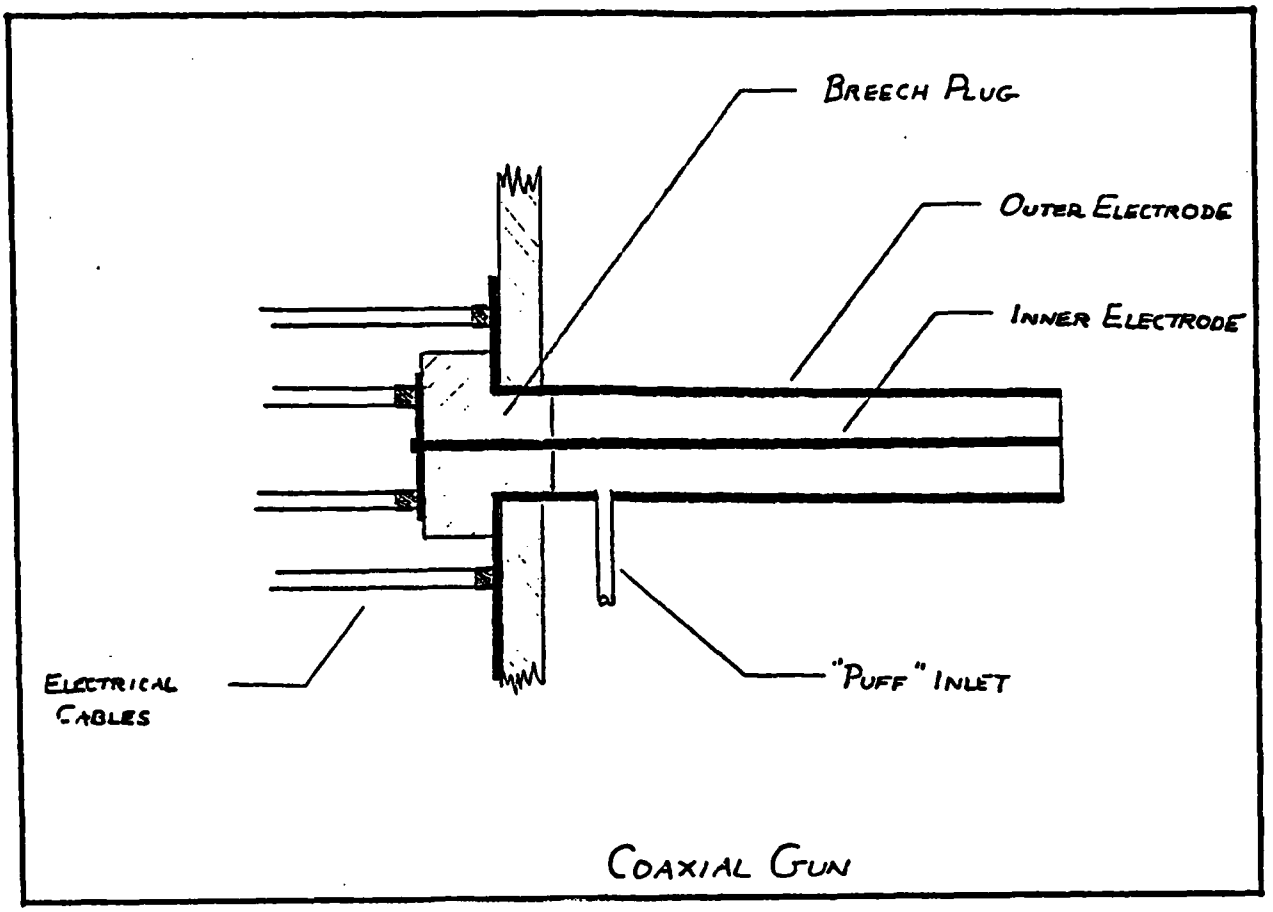

FIGURE 7a

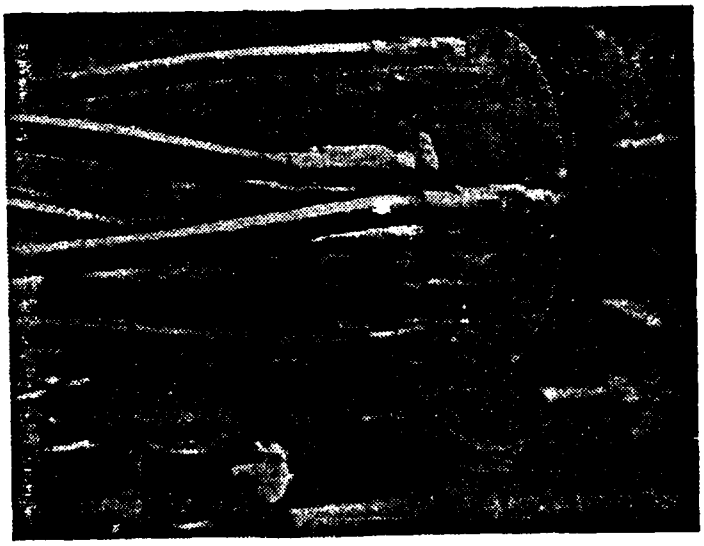

FIGURE 7b

FIGURE 8

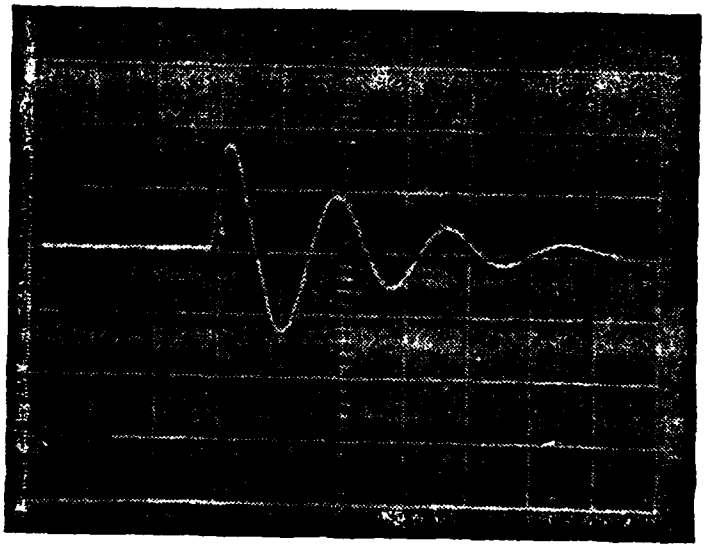

FIGURE 9

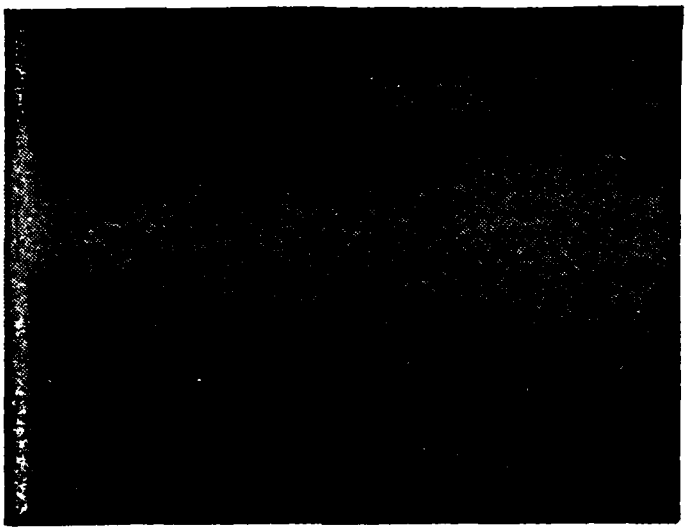

FIGURE 10

are visible in Figures 6a and 6b. The coils consist of 4 turns each and are 145 cm long, 30 cm wide and are separated by 25 cm. The array has an effective inductance of approximately 100 uh. The array is powered by a capacitor bank comprised of 4 capacitors in parallel each rated at 60 μf and 20 KV. The bank is switched by 4 type GL-7703 ignitrons in parallel. The calculated field profiles (normalized to the

field at the array center) are plotted in Figures 11a and 11b for the orientation: x, width; y, length; z, separation. Figure 12 shows the array location on the vacuum chamber. The capacitor bank "dumps" into the array with a pulse (critically damped) that peaks in 200 μsec and zeroes in 500 μsec. Figure 13 shows a typical field signal as picked up by a magnetic field probe at the array center. With 3 KV on the bank, the field at the center is measured to be approximately 0.05 weber/m^2 (500 gauss). The field is proportional to the bank charge voltage over a large range of initial charge. An estimate of the fields required to operate in the $M_A >> 1$ regime is calculated in Appendix 1.

3. The Vacuum Chamber and Pumps - The vacuum chamber is constructed out of 6" diameter Corning pyrex sanitary drain pipe sections with rubber gaskets. Figure 14 shows the overall dimensions of the chamber. The gun is mounted on the axis of the "T" end. The chamber is pumped by a large, two-stage mechanical pump (Welsh 1397) and a small oil diffusion pump with backing pump to the 1-10 uHg range.

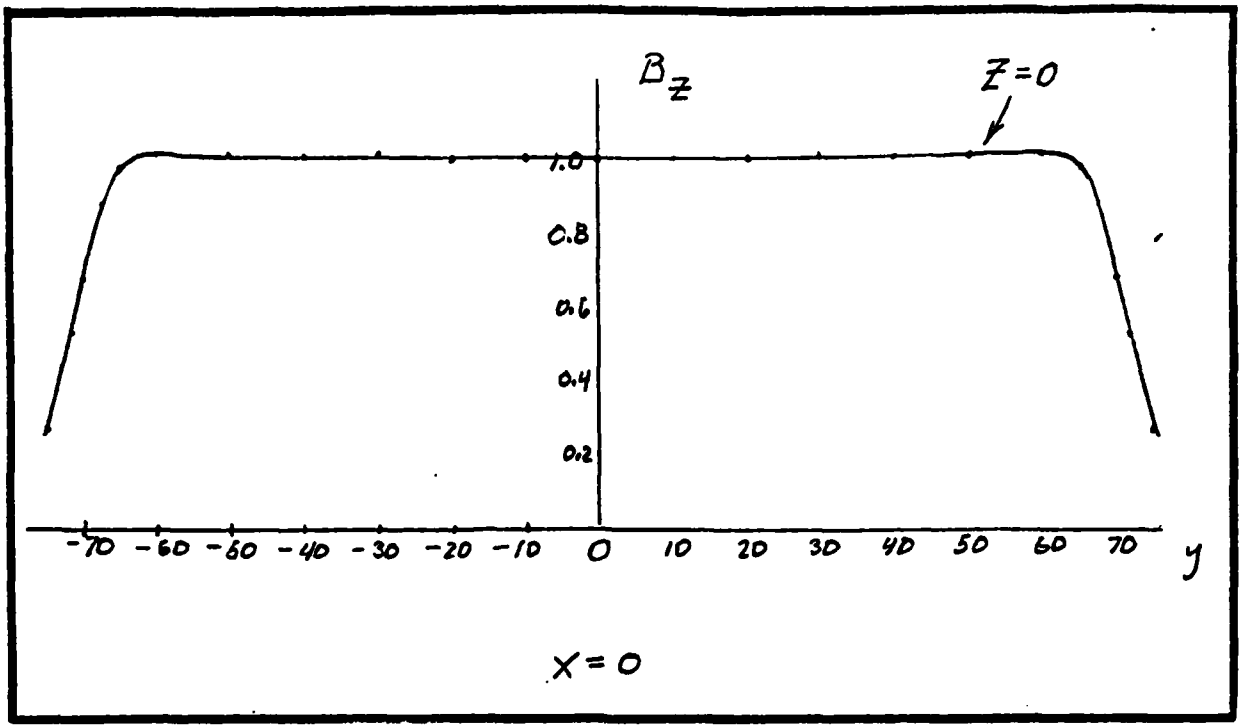

FIGURE 11a

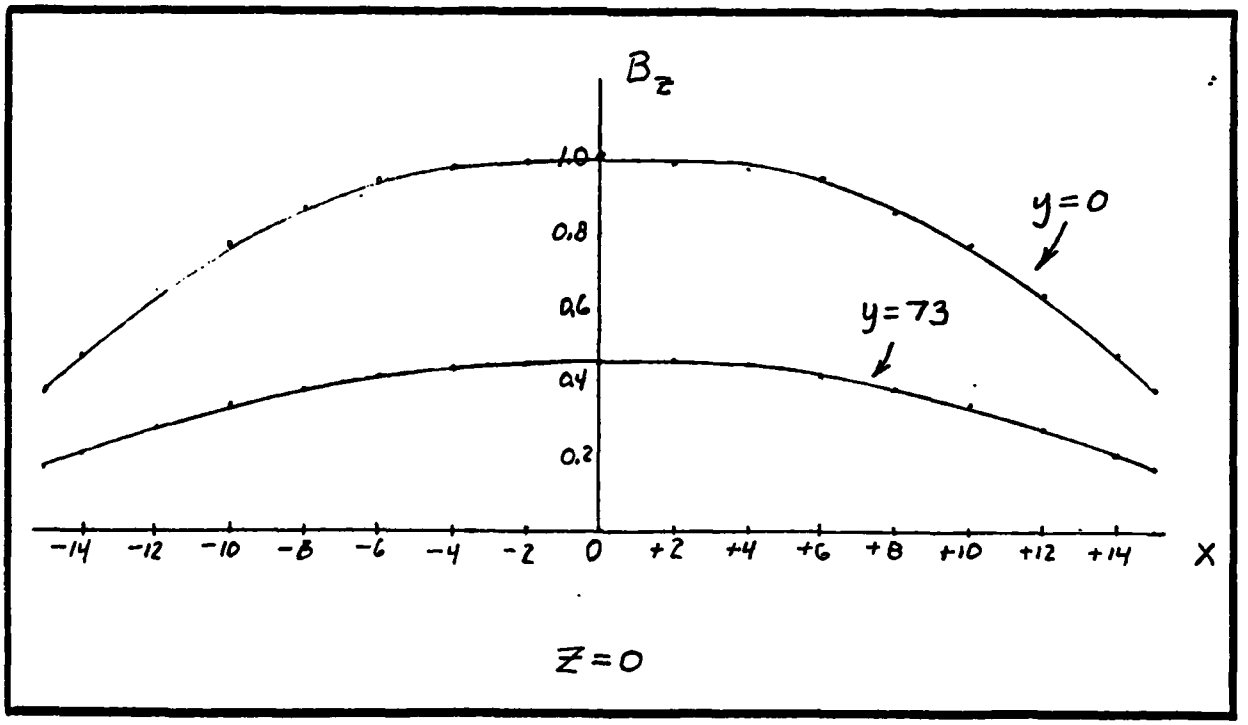

FIGURE 11b

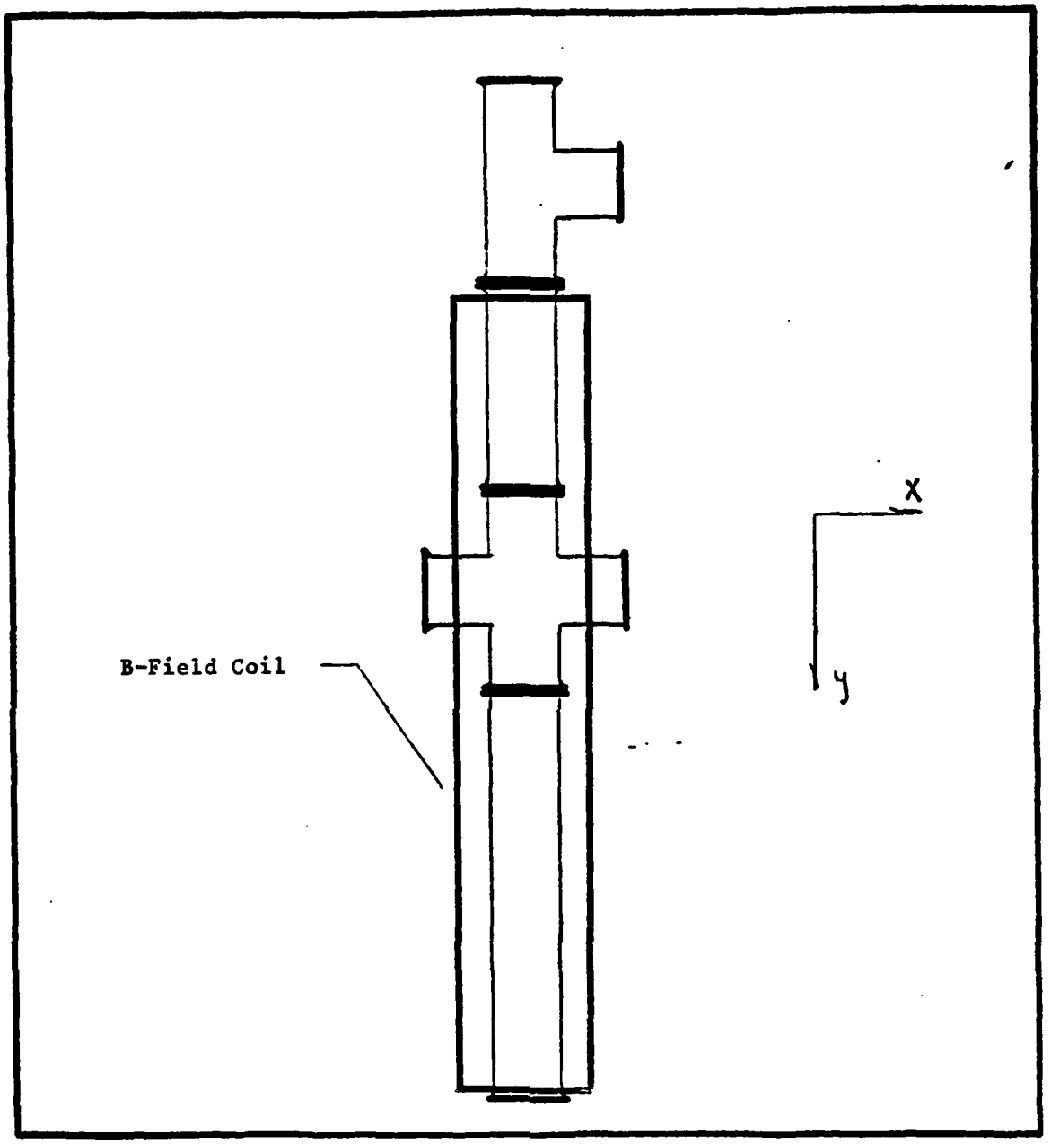

FIGURE 12

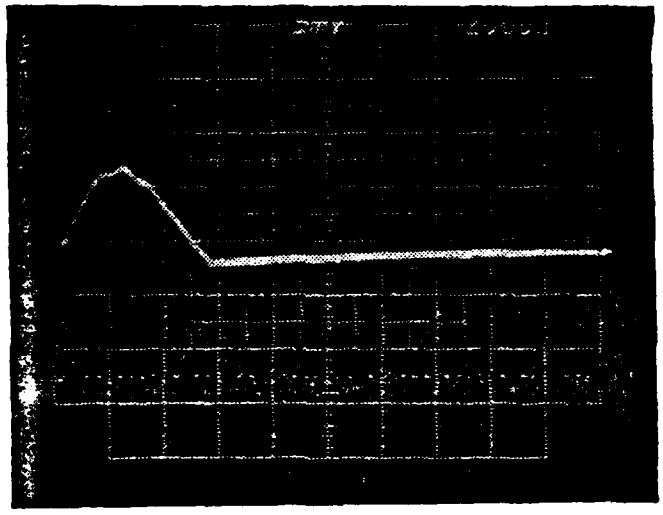

FIGURE 13

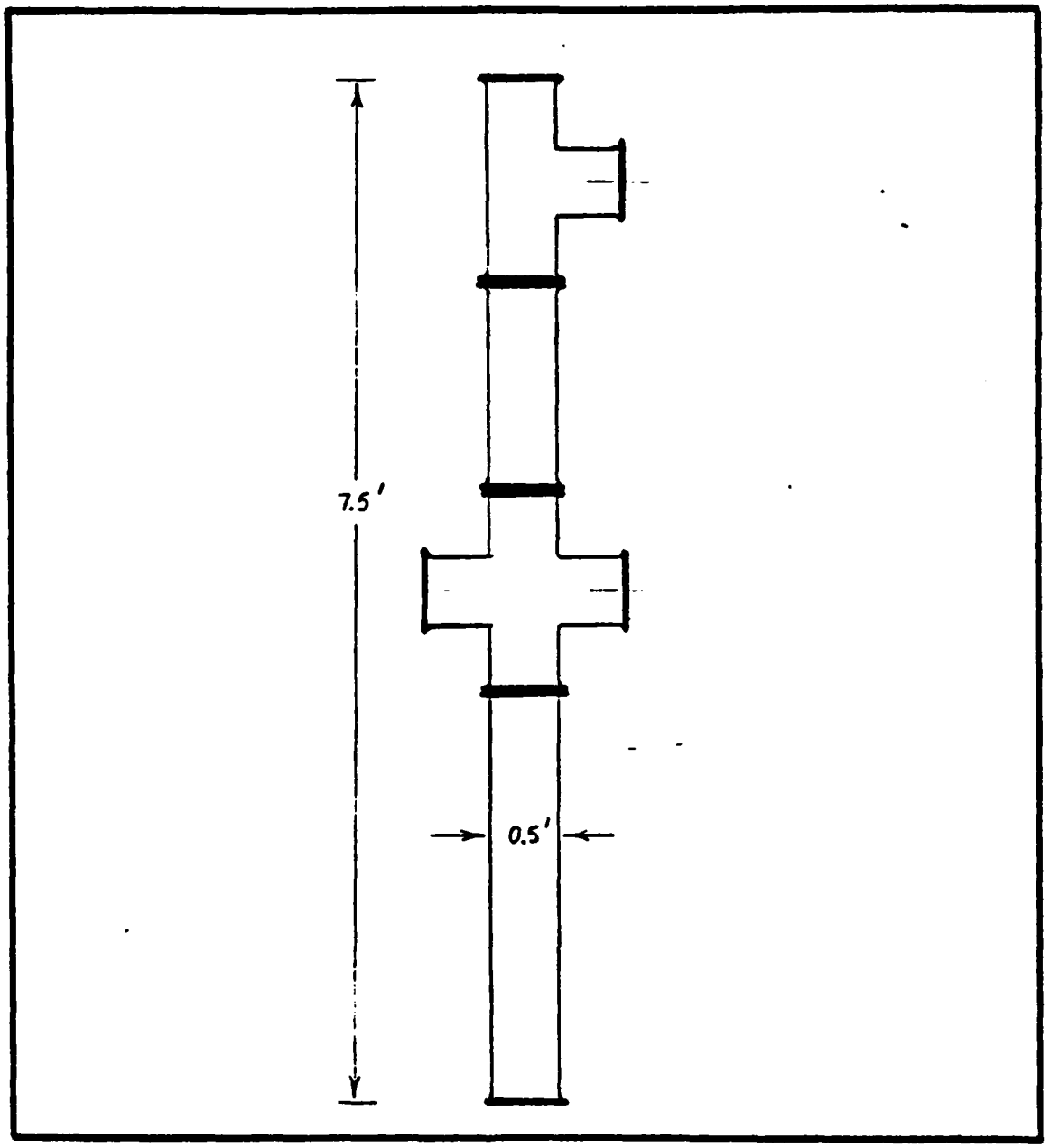

FIGURE 14

4. Plasma and Field Diagnostics - The background and short time-scale magnetic fields are measured by magnetic probes connected to passive RC integrators. Figure 15 shows such a probe inserted through an access port into a crossed-T section. A typical calibration for such a probe working into a 100 μsec RC integrator is 0.5 mV/gauss (5 V/weber/m^2).

The plasma velocity is measured by "time-of-flight" techniques using a bifurcated light pipe and a very fast response photodiode detector (Tropel). Figure 16 shows the setup and Figure 17 shows the location of the velocity probe as well as the field probe on the chamber.

The density gradient structure of the beam is measured by a laser schliren system (Kiefer & Lutz, 1965) with a 2 m travel path and using a 5 mwatt helium-neon laser as a source. The geometry of the setup is shown in Figure 18 and portions of the actual system are shown in Figures 19a, 19b, and 19c. In this system the voltage from the photodiode detector is proportional to the plasma (local) density gradient.

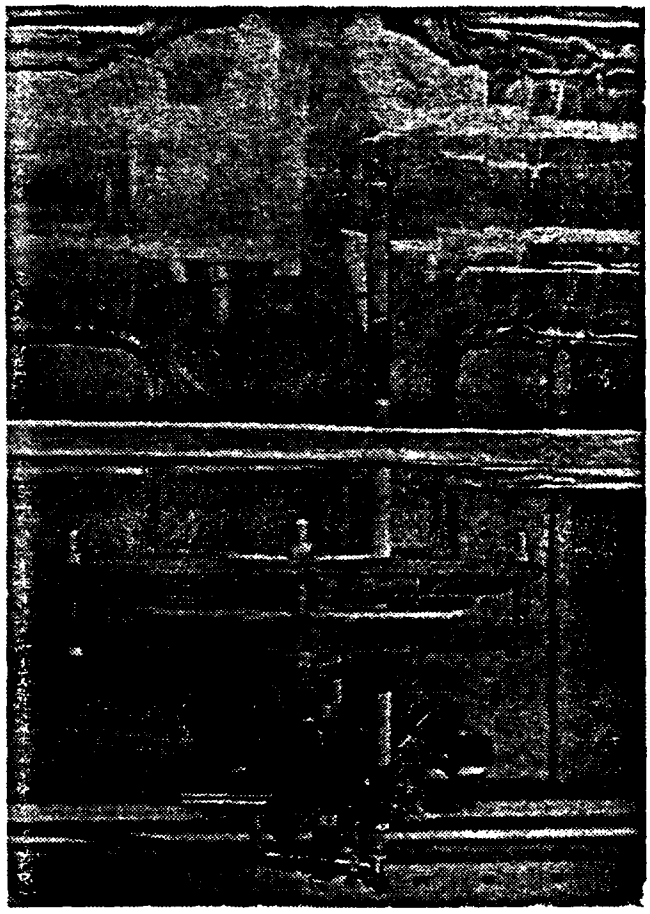

FIGURE 15

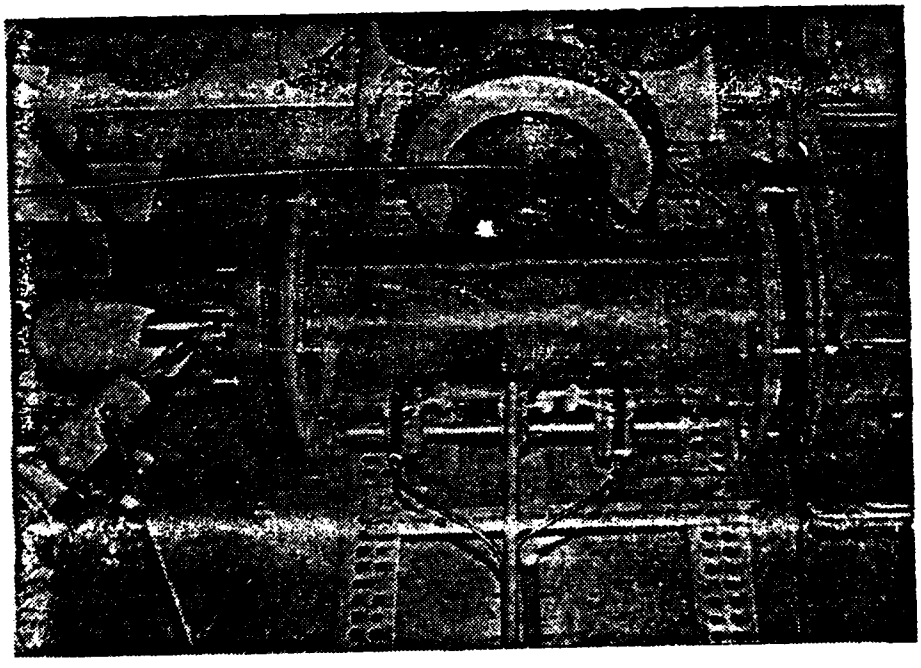

FIGURE 16

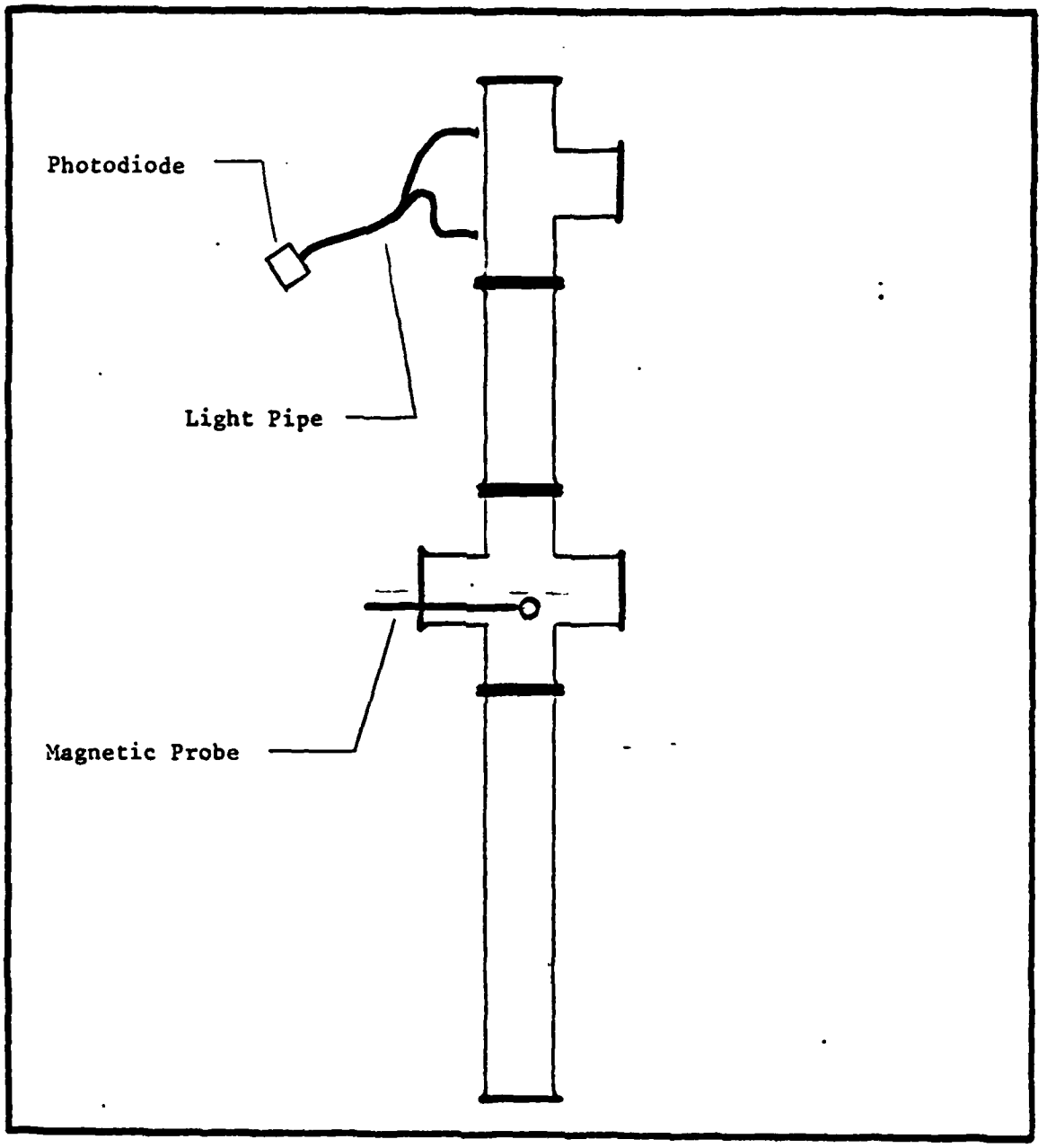

FIGURE 17

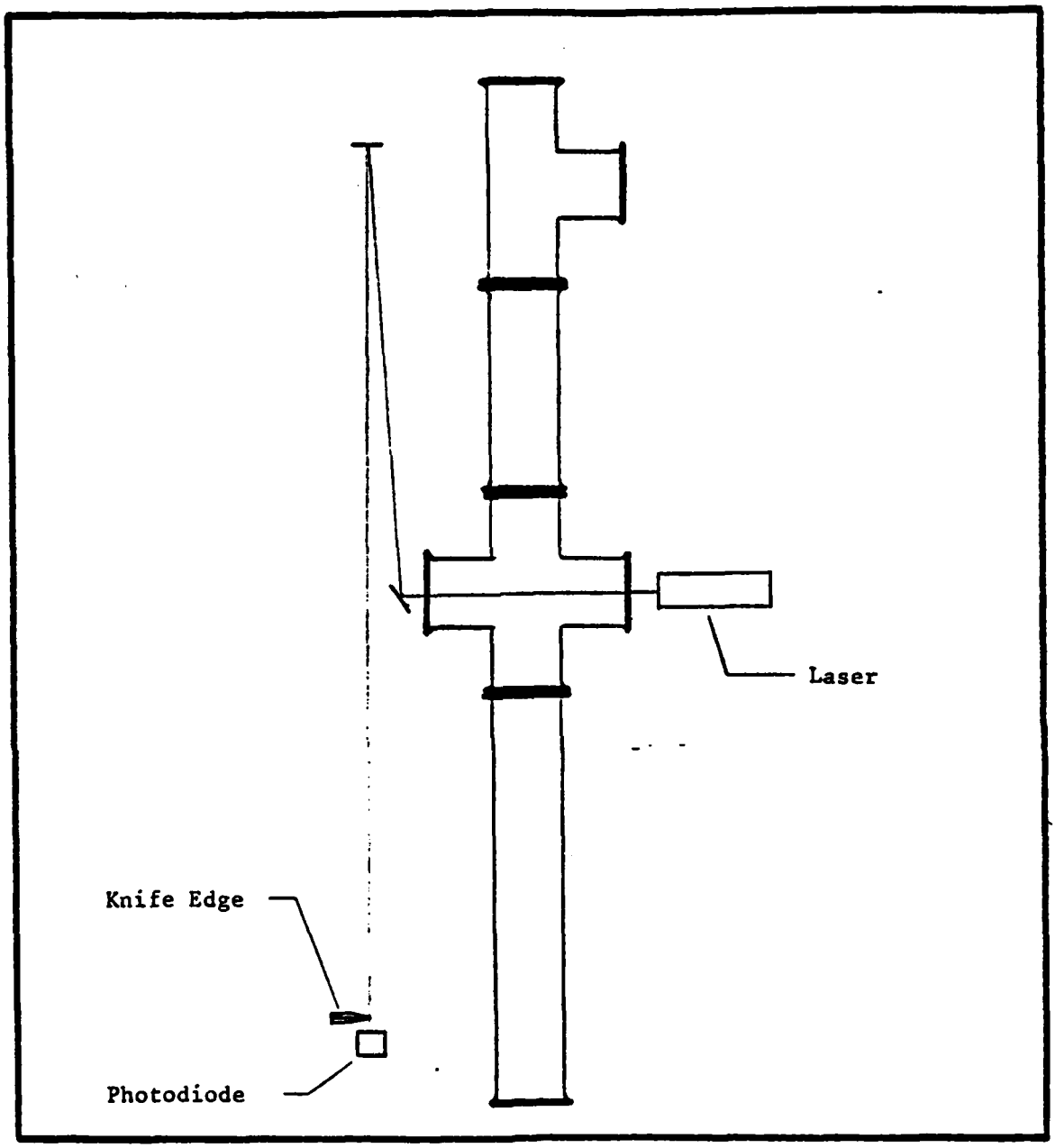

FIGURE 18

FIGURE 19a

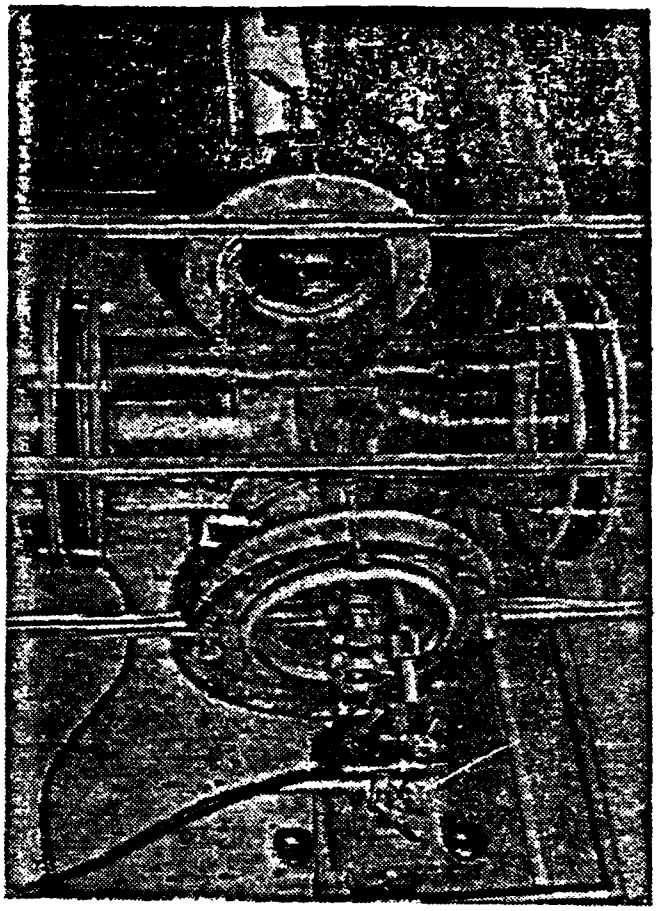

Figure 19b

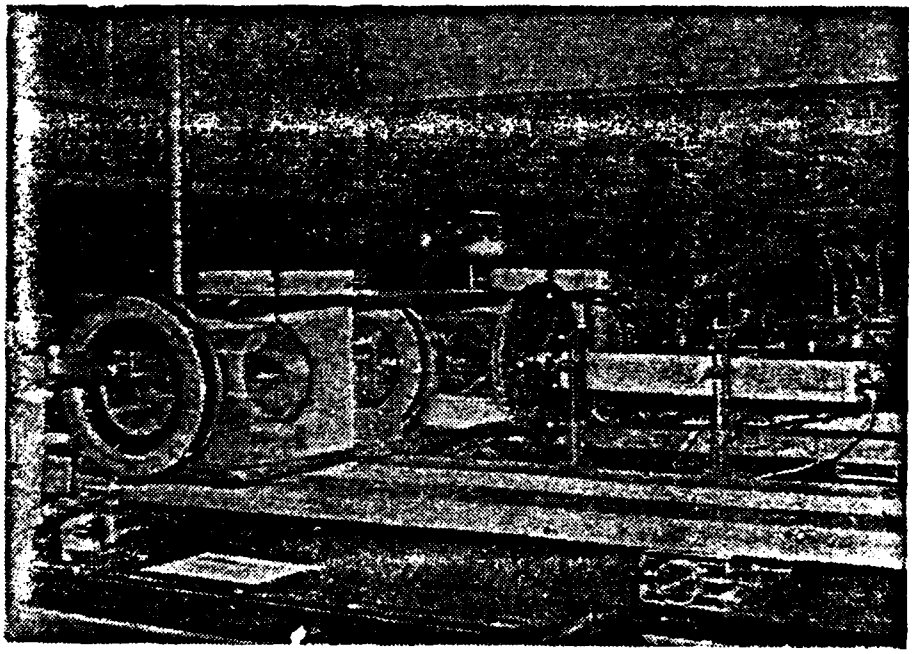

FIGURE 19c

A fast optical Kerr cell shutter system has been designed and constructed but is not yet operative. This system will be used to obtain very short time interval photographs (100 nsec) which will catch the beam at early times in its propagation and allow for analysis of the mode structure of any dynamic instabilities.

5. The Data Acquisition/Control Room - The control room is completely enclosed by a double screen shielded room. Figure 20 shows the back of that enclosure and the BNC data/signal ports. The control room instrumentation includes 4 Tektronix storage oscilloscopes (Figure 21a) for data monitoring. Precisely controllable trigger signals are generated by the combination of a Tektronix 161/162 signal generator and an Abtronics Model 100 4 channel time delay generator (Figure 21b).

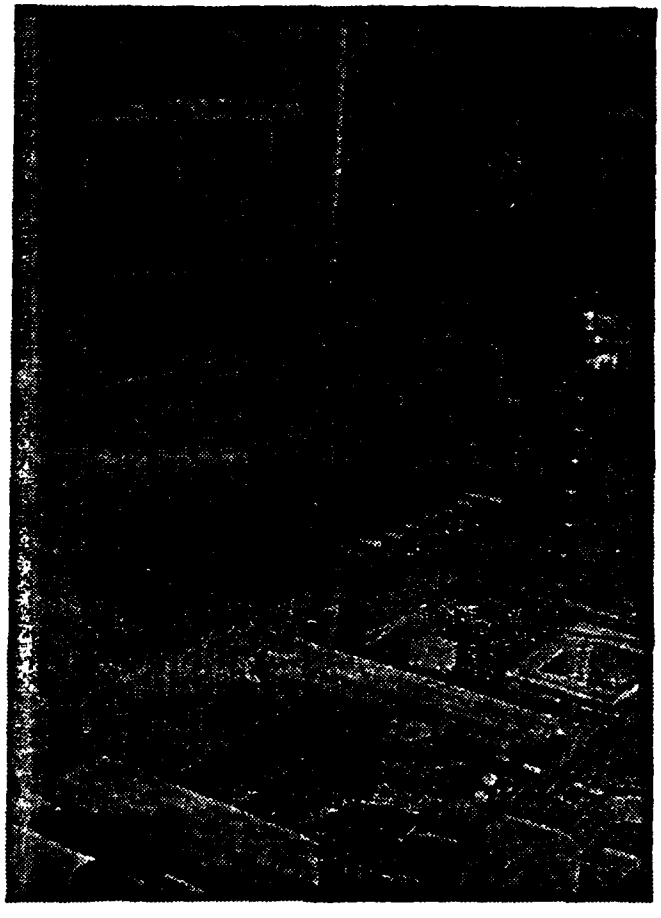

FIGURE 20

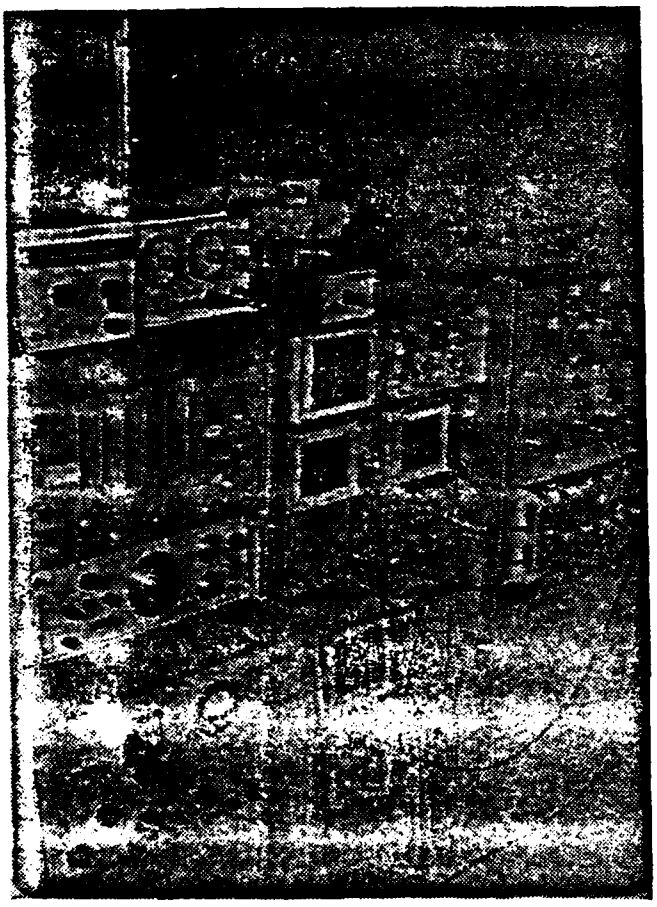

FIGURE 21a

FIGURE 21b

6.0 STATUS OF THE THEORETICAL EFFORT

This section presents results of the theoretical effort concerned with the analytic solution for the dynamic magnetic field response within the plasmoid wake, precursor and slab regions. Two cases are presented as follows:

Case 1: Includes inertial effects while excluding polarization and collisional effects.

Case 2: Includes inertial and collisional effects while excluding polarization effects.

Case 1 essentially describes and/or simulates the conditions inherent in the W.R. Shanahan formalism of plasmoid propagation across a magnetic field. In this case, the solution for the dynamic magnetic field response within the various plasmoid regions exhibits a secular behavior. It is our contention this is an erroneous behavior.

Case 2 addresses and attempts to resolve the secularity issue by introducing a collisional term proportional to the collision frequency (ν_{ei}) between electrons and ions. The collision term introduces a dissipative mechanism which leads to exponential damping of inertial plasma oscillations. It is our contention that in this case, the secular behavior of the dynamic magnetic field response will no longer be erroneously exhibited.

Before presenting the detailed analytics of Case 1 and Case 2, it should be pointed out that our formalism attempts to address several critical issues which play a dominant role in analyzing plasmoid propagation across a magnetic field. These issues are; multi-dimensionality, collisions between species (e,i), transverse and longitudinal polarization, plasmoid deceleration due to interactions with the polarization fields, and the many mechanisms which lead to the redirection of longitudinal motion to transverse motion, which in turn, leads to catastrophic disruption of the plasmoid beam over the time scale of propagation.

It now becomes necessary to point out that the W.R. Shanahan formalism, based upon the conservation of canonical angular momentum, which in fact is not conserved, neglects electrostatic polarization fields in the analytic treatment while simultaneously incorporating those fields in the numerical particle-in-cell simulations. Likewise, the Sinel'nikov and Rutkevich formalism considered to be more comprehensive than the Peter and Rostoker formalism, assumes a steady state ($\partial/\partial t \rightarrow 0$) in the equations of motion for electrons and ions. Also, the Sinel'nikov and Rutkevich formalism does not include a collisional exchange term in the momentum balance equations of motion. The results of our analytic formalism is presented as follows:

Case 1: Includes inertial effects, excludes polarization and collisional effects.

Simplified ohms law:

$$\underline{E} + \underline{V} \times \underline{B} = \frac{1}{\epsilon_0 \omega_{pe}^2} \frac{\partial \underline{J}}{\partial t} \tag{1}$$

Maxwell's Equations:

$$\vec{\nabla} \times \underline{B} = -\nabla^2 \underline{A} = \mu_0 \underline{J} + \mu_0 \epsilon_0 \frac{\partial \underline{E}}{\partial t} \tag{2}$$

$$\vec{\nabla} \times \underline{E} = -\frac{\partial \underline{B}}{\partial t} \rightarrow \underline{E} = -\frac{\partial \underline{A}}{\partial t} \tag{3}$$

Combining Equations (1), (2), and (3) we have:

$$\nabla^2 \underline{A} - \frac{1}{c^2} \frac{\partial^2 \underline{A}}{\partial t^2} = -\mu_0 \underline{J} \tag{4}$$

$$\frac{1}{\epsilon_0 \omega_{pe}^2} \frac{\partial \underline{J}}{\partial t} = -\frac{\partial \underline{A}}{\partial t} + \vec{V} \times \vec{B} \tag{5}$$

PLASMOID PROPAGATION GEOMETRY

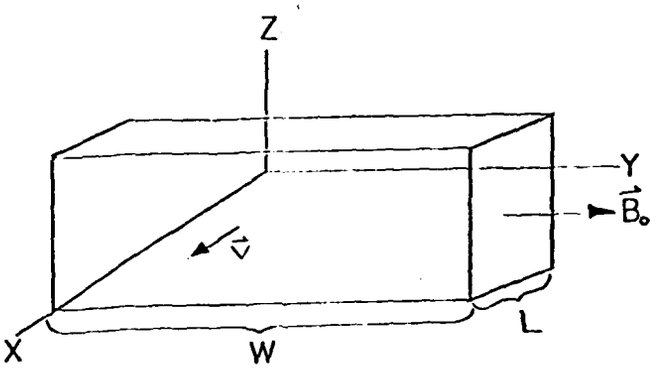

FIGURE 22.

Assume:

$$\rho = \rho(x) \;,\quad \vec{v} = v_o\,\hat{x} \;,\quad \vec{B}_o = B_o\,\hat{y} \;,\quad \vec{J} = J_z\,\hat{z}$$

Therefore, from equations (4) and (5) we have:

$$\nabla^2 A_z - \frac{1}{c^2}\frac{\partial^2 A_z}{\partial t^2} = -\mu_o J_z \qquad (6)$$

$$\frac{1}{\epsilon_o \omega_{pe}^2}\frac{\partial J_z}{\partial t} = -\frac{\partial A_z}{\partial t} + v_o B_o \qquad (7)$$

LAB Frame:

$$X < V_0 t : \quad \left(\frac{\partial^2}{\partial x^2} + \frac{\partial^2}{\partial y^2} - \frac{1}{c^2}\frac{\partial^2}{\partial t^2}\right) A_z = 0 \tag{8}$$

$$V_0 t \le x \le V_0 t + L : \left(\frac{\partial^2}{\partial x^2} + \frac{\partial^2}{\partial y^2} - \frac{1}{c^2}\frac{\partial^2}{\partial t^2}\right) A_z = \frac{\omega_p^2}{c^2} A_z + \frac{\omega_p^2}{c^2} B_0 (x - V_0 t) \tag{9}$$

$$x > V_0 t + L : \left(\frac{\partial^2}{\partial x^2} + \frac{\partial^2}{\partial y^2} - \frac{1}{c^2}\frac{\partial^2}{\partial t^2}\right) A_z = 0 \tag{10}$$

Also: $$A_z(x,y,t)\Big|_{t=0} = -x B_0 \ , \quad \frac{\partial A_z(x,y,t)}{\partial t}\Big|_{t=0} = 0 = -E_z(x,y,t)\Big|_{t=0}$$

Transformation:

$$x' = \frac{x - V_0 t}{\sqrt{1 - V_0^2/c^2}} \ , \quad t' = \frac{t - \frac{V_0}{c^2} x}{\sqrt{1 - V_0^2/c^2}} \ , \quad y' = y$$

$$A_z \to A_z' \ , \quad E_z' = \frac{E_z + V_0 B_0}{\sqrt{1 - V_0^2/c^2}}$$

$$\therefore \left(\frac{\partial^2}{\partial x^2} + \frac{\partial^2}{\partial y^2} - \frac{1}{c^2}\frac{\partial^2}{\partial t^2}\right) A_z \to \left(\frac{\partial^2}{\partial x'^2} + \frac{\partial^2}{\partial y^2} - \frac{1}{c^2}\frac{\partial^2}{\partial t'^2}\right) A_z'$$

$$= \frac{\omega_p^2}{c^2} A_z' + \frac{\omega_p^2}{c^2} B_0 x' \sqrt{1 - V_0^2/c^2} \quad : \ V_0 t \le x \le V_0 t + L$$

Boundaries:

$$x - v_0 t = 0 \rightarrow x' = 0$$
$$x - v_0 t = L \rightarrow x' = \frac{L}{\sqrt{1 - v_0^2/c^2}}$$

Boundary Conditions:

$$A'_z \Big|_{x'<0} \equiv A'_{wake}, \quad A'_z \Big|_{x'>L} \equiv A'_{Precursor}, \quad A'_z \Big|_{0 \le x \le L} \equiv A'_{slab}$$

$$\therefore \quad A'_{wake} \Big|_{x'=0} = A'_{slab} \Big|_{x'=0}, \quad A'_{slab} \Big|_{x'=L} = A'_{precursor} \Big|_{x'=L}$$

Also Since $B'_y = -\frac{\partial}{\partial x'} A'_z$, we have:

$$B'_{y_{wake}} = -\frac{\partial}{\partial x'} A'_{z_{wake}}, \quad B'_{y_{slab}} = -\frac{\partial}{\partial x'} A'_{z_{slab}}, \quad B'_{y_{precursor}} = -\frac{\partial}{\partial x'} A'_{z_{precursor}}$$

$$\therefore \quad \frac{\partial}{\partial x'} A'_{z_{wake}} \Big|_{x'=0} = \frac{\partial}{\partial x'} A'_{z_{slab}} \Big|_{x'=0}, \quad \frac{\partial}{\partial x'} A'_{z_{slab}} \Big|_{x'=L/\sqrt{1-v_0^2/c^2}} = \frac{\partial}{\partial x'} A'_{z_{precursor}} \Big|_{x'=L/\sqrt{1-v_0^2/c^2}}$$

Initial Conditions: Note: $B'_y = \frac{B_y + \frac{v_0}{c^2} E_z}{\sqrt{1 - v_0^2/c^2}}$

$$E_z = -\frac{\partial A_z}{\partial t}, \quad B_y \Big|_{t=0} = B_0, \quad A_z \Big|_{t=0} = -x B_0$$

Now Assume:

$$B'_y\Big|_{t'=0} = \text{Constant in Space}, \quad E_z\Big|_{t=0} = 0$$

$$\therefore \quad B'_y\Big|_{t=0} = \frac{B_0}{\sqrt{1-V_0^2/c^2}}, \quad B'_y\Big|_{x,t=0} = \frac{B_0}{\sqrt{1-V_0^2/c^2}} = B'_y\Big|_{x',t'=0}$$

And Consistently:

$$A'_z\Big|_{t'=0} = \frac{-x' B_0}{\sqrt{1-V_0^2/c^2}}$$

Now Since:

$$E'_z = \frac{E_z + V_0 B_0}{\sqrt{1-V_0^2/c^2}}, \text{ we have:}$$

$$-\frac{\partial}{\partial t'} A'_z = -\frac{\frac{\partial A_z}{\partial t} + V_0 B_0}{\sqrt{1-V_0^2/c^2}}$$

Then:

$$-\frac{\partial}{\partial t'} A'_z\Big|_{t=0} = \frac{V_0 B_0}{\sqrt{1-V_0^2/c^2}} = \text{constant in Space} = -\frac{\partial}{\partial t'} A'_z\Big|_{x,t=0}$$

$$\therefore \quad \frac{\partial}{\partial t'} A'_z\Big|_{t'=0} = -\frac{V_0 B_0}{\sqrt{1-V_0^2/c^2}}$$

Consider plasmoid wake and precursor regions:

$$\left(\frac{\partial^2}{\partial x'^2} + \frac{\partial^2}{\partial y'^2} - \frac{1}{c^2}\frac{\partial^2}{\partial t'^2}\right) A'_z = 0 \qquad (11)$$

Taking the Laplace transform of equation (8)

Where:

$$\mathcal{L}(A_z) \equiv \mathcal{A}_z$$

We have:

$$\left(\frac{\partial^2}{\partial x'^2} + \frac{\partial^2}{\partial y'^2} - \frac{1}{c^2}\frac{\partial^2}{\partial t'^2}\right) A'_z \rightarrow \left(\frac{\partial^2}{\partial x'^2} + \frac{\partial^2}{\partial y'^2} - \frac{s^2}{c^2}\right)\mathcal{A}'_z - \frac{1}{c^2}\left(-sA'_z\Big|_{t'=0} - \frac{\partial}{\partial t'}A'_z\Big|_{t'=0}\right) \qquad (12)$$

$$\therefore \left(\frac{\partial^2}{\partial x'^2} + \frac{\partial^2}{\partial y'^2} - \frac{s^2}{c^2}\right)\mathcal{A}'_z = \frac{1}{c^2}\frac{sx'B_0}{\sqrt{1-v_0^2/c^2}} + \frac{1}{c^2}\frac{v_0 B_0}{\sqrt{1-v_0^2/c^2}} \qquad (13)$$

REMARKS CONCERNING THE ANALYTIC SOLUTION OF EQUATION (13)

The analytic solution of equation (13) for the plasmoid wake and precursor regions describes electromagnetic plane waves, originating within the plasmoid slab, which propagate into the wake and precursor regions at the speed of light. The amplitude (constant) of the plane waves is dependent upon initial conditions within the plasmoid slab region.

Although the actual analytic solution of equation (13) is not presented herein due to mathematical uncertainties, it can be stated that is our contention, the analytic solu-

tion for the dynamic magnetic field response within our context (Wake, Precursor Regions) exhibits an erroneous secular behavior if solved by conventional techniques. Note that the analytic solution for the dynamic magnetic field response as presented by W.R. Shanahan (Section 4.0) also exhibits secular behavior.

Specifically, if the general solution of the second order nonhomogenous differential equation (13) is represented as the sum of a particular solution A_p and a complementary solution A_H, it can be shown that the general solution of equation (13) for the transformed magnetic vector potential (A_{zwake}, $A_{zprecursor}$) will exhibit secular growth. The dynamic magnetic field response, obtained by performing the vector curl of the magnetic vector potential, also exhibits secular growth. Note that the nonhomogenous terms (initial conditions) of equation (13) arise from performing the Laplace transform of equation (11) which contains a second order partial derivative in time and if these nonhomogenous terms are treated as driver terms, an erroneous solution will be obtained.

Consider plasmoid slab region: $0 \leq x' \leq \frac{L}{\sqrt{1-v_0^2/c^2}}$

$$\therefore \left(\frac{\partial^2}{\partial x'^2} + \frac{\partial^2}{\partial y^2} - \frac{1}{c^2}\frac{\partial^2}{\partial t'^2}\right) A'_{z_{slab}} - \frac{1}{c^2}\omega_p^2 A'_{z_{slab}} = \frac{\omega_p^2}{c^2} B_0 x' \sqrt{1-v_0^2/c^2} \qquad (14)$$

Taking the Laplace transform of equation (11) we have:

$$\left(\frac{\partial^2}{\partial x'^2}+\frac{\partial^2}{\partial y'^2}-\frac{s^2}{c^2}\right)\mathcal{A}_{z_{slab}}-\frac{1}{c^2}\left(-sA'_{z}\Big|_{\substack{slab\\ t'=0}}-\frac{\partial}{\partial t'}A'_{z}\Big|_{\substack{slab\\ t'=0}}\right)-\frac{\omega_p^2}{c^2}\mathcal{A}_{z_{slab}}=\frac{1}{s}\frac{\omega_p^2}{c^2}B_o x'\sqrt{1-v_o^2/c^2} \qquad (15)$$

OR:

$$\left(\frac{\partial^2}{\partial x'^2}+\frac{\partial^2}{\partial y'^2}-\frac{1}{c^2}(s^2+\omega_p^2)\right)\mathcal{A}_{z_{slab}}=\frac{1}{c^2}\left(\frac{sx'B_o}{\sqrt{1-v_o^2/c^2}}+\frac{v_o B_o}{\sqrt{1-v_o^2/c^2}}\right)+\frac{1}{s}\frac{\omega_p^2}{c^2}B_o x'\sqrt{1-v_o^2/c^2} \qquad (16)$$

REMARKS CONCERNING THE ANALYTIC SOLUTION OF EQUATION (16)

The analytic solution of equation (16) for the plasmoid slab region describes electromagnetic plane waves bouncing back and forth within the slab region at a phase velocity greater than the speed of light. The group velocity, however, cannot exceed the speed of light. The dispersion relation for electromagnetic plane waves propagating within the plasmoid slab differs from the dispersion relation for electromagnetic plane waves propagating in the plasmoid wake and precursor regions, by two terms containing ωp^2 reminiscent of inertial plasma oscillations. These terms in the dispersion relation, as can be seen by referring to equation (9), are due to a driver term characteristic of the plasmoid current density ($\mu_o J_z$). It should be pointed out that the two models of (Peter and Rostoker) and Sinel'nikov and Rutkevich) exhibit exactly these same inertial plasma oscillations (Refer to Figure 22).

Case 2: Includes inertial and collisional effects, excludes polarization effects

Simplified ohms law:

$$\underline{E} + \underline{V} \times \underline{B} = \frac{1}{\epsilon_0 \omega_{pe}^2} \left[\frac{\partial \underline{J}}{\partial t} + \nu_{ei} \underline{J} \right] \tag{1}$$

Maxwell's equations:

$$\vec{\nabla} \times \vec{B} = -\nabla^2 \underline{A} = \mu_0 \underline{J} + \mu_0 \epsilon_0 \frac{\partial \underline{E}}{\partial t} \tag{2}$$

$$\vec{\nabla} \times \underline{E} = -\frac{\partial \underline{B}}{\partial t} \rightarrow \underline{E} = -\frac{\partial \underline{A}}{\partial t} \tag{3}$$

Combining equations (1), (2), and (3) we have:

$$\nabla^2 \underline{A} - \frac{1}{c^2} \frac{\partial^2 \underline{A}}{\partial t^2} = -\mu_0 \underline{J} \tag{4}$$

$$\frac{1}{\epsilon_0 \omega_{pe}^2} \left[\frac{\partial \underline{J}}{\partial t} + \nu_{ei} \underline{J} \right] = -\frac{\partial \underline{A}}{\partial t} + \vec{V} \times \vec{B}$$

Using the same plasmoid propagation geometry, we have:

$$\vec{\nabla}^2 A_z - \frac{1}{c^2}\frac{\partial^2 A_z}{\partial t^2} = -\mu_0 J_z \tag{5}$$

$$\frac{1}{\epsilon_0 \omega_{pe}^2}\left[\frac{\partial J_z}{\partial t} + \nu_{ei} J_z\right] = -\frac{\partial A_z}{\partial t} + V_0 B_0 \tag{6}$$

Consider the plasmoid wake and precursor regions:

$$\therefore \left(\frac{\partial^2}{\partial x'^2} + \frac{\partial^2}{\partial y^2} - \frac{1}{c^2}\frac{\partial^2}{\partial t'^2}\right) A_z' = 0 \tag{7}$$

Taking the Laplace transform of equation (7), we have:

$$\left(\frac{\partial^2}{\partial x'^2} + \frac{\partial^2}{\partial y^2} - \frac{s^2}{c^2}\right) A_z' = \frac{1}{c^2}\frac{s x' B_0}{\sqrt{1 - V_0^2/c^2}} + \frac{1}{c^2}\frac{V_0 B_0}{\sqrt{1 - V_0^2/c^2}} \tag{8}$$

The solution of equation (8) for the transformed magnetic vector potential is identical to that discussed in Case 1 for the wake and precursor regions. Specifically, electromagnetic plane waves propagating at the speed of light into the wake and precursor regions.

Consider the plasmoid slab region: $0 \leq x' \leq \frac{L}{\sqrt{1-v_0^2/c^2}}$

$$\left(\frac{\partial^2}{\partial x'^2} + \frac{\partial^2}{\partial y^2} - \frac{s^2}{c^2}\right) A_{z_{slab}} - \frac{1}{c^2}\left(-s A'_{z_{slab}}\Big|_{t'=0} - \frac{\partial}{\partial t'} A'_{z_{slab}}\Big|_{t'=0}\right) = -\mu_0 \mathcal{J}_z \qquad (9)$$

Where: $\mathcal{L}(J_z) \equiv \mathcal{J}_z$

Equation (9) can be rewritten as:

$$\left(\frac{\partial^2}{\partial x'^2} + \frac{\partial^2}{\partial y^2} - \frac{s^2}{c^2}\right) A'_{z_{slab}} - \frac{1}{c^2}\frac{s x' B_0}{\sqrt{1-v_0^2/c^2}} - \frac{1}{c^2}\frac{v_0 B_0}{\sqrt{1-v_0^2/c^2}} = -\mu_0 \mathcal{J}_z \qquad (10)$$

Taking the Laplace Transform of equation (6) and solving for J_z

We have:

$$\left(\frac{\partial^2}{\partial x'^2} + \frac{\partial^2}{\partial y^2} - \frac{1}{c^2}\left(s^2 + \frac{\omega_p^2 s}{(s+\nu_{ei})}\right)\right) A'_{z_{slab}} = \frac{1}{c^2}\left(\frac{s x' B_0}{\sqrt{1-v_0^2/c^2}} + \frac{v_0 B_0}{\sqrt{1-v_0^2/c^2}} + \frac{\omega_p^2 B_0 x' \sqrt{1-v_0^2/c^2}}{s+\nu_{ei}}\right) \qquad (11)$$

REMARKS CONCERNING THE ANALYTIC SOLUTION OF EQUATION (11)

The analytic solution of equation (11) for the transformed magnetic vector potential is similar to that discussed in Case 1 for the plasmoid slab region except that a dissipative term has been introduced. The effect of the dissipative term is to damp the inertial plasma oscillations.

The dynamic magnetic field response, obtained by performing the vector curl of the magnetic vector potential (A_z), does not exhibit secular behavior in this case. Again, the actual analytic solutions are not presented herein due to mathematical incertainties.

BIBLIOGRAPHY

1. Ferraro, V.C.A., "On the Theory of the First Phase of A Geomagnetic Storm: A New Illustrative Calculation Based on Idealized (Plane not Cylindrical) Model Field Distribution," J. Geophys. Res. 57, 15 (1952).

2. Spitzer, L., Physics of Fully Ionized Gases, Interscience Tracts on Physics and Astronomy, 3, Interscience Publishers (1962).

3. Okhawa, T., Nucl, Fusion 10, 185 (1970).

4. Ott, E. and Manheimer, W.M., Nucl. Fusion 17, 1057 (1977).

5. Peter, W., Ph.D. Dissertation, University of California, Irvine (1981).

6. Schmidt, G., Phys. Fluids 3, 961 (1960).

7. Los Alamos Scientific Laboratory, "Preliminary Considerations Concerning Neutral Plasma Beam Propagation Across A Magnetic Field," LA-7954-MS/UC-34(1979).

8. Peter, W. and Rostoker, N., "Theory of Plasma Injection Into A Magnetic Field," Phys. Fluids 25 (4), 730 (1982).

9. Sinel'nikov, K.D. and Rutkevich, B.N., "A Bounded Plasma Flux in a Magnetic Field," Sov. Phys.-Tech. Phys 12(1), 37 (1967).

APPENDIX 1

COMPUTATION OF MAGNETIC FIELD LIMIT

COMPUTATION OF MAGNETIC FIELD LIMIT:

CRITERION: $V/V_A \geq 10$

where V = PLASMA FLOW VELOCITY

V_A = ALFVEN SPEED

$= B/(\mu_0 MN)^{\frac{1}{2}}$

B = MAGNETIC FIELD STRENGTH

M = PLASMA PARTICLE MASS

N = PLASMA PARTICLE DENSITY

$\therefore B \leq V (\mu_0 MN)^{\frac{1}{2}}/10$

In MKS Units: $\mu_0 \sim 10^{-6}$

$M \sim 10^{-26}$

$N \sim 10^{22}$

$V \sim 10^{4}$

$\therefore B \leq 10^{-2}$ (10^{2} GAUSS)

END

FILMED

3-85

DTIC